Adapting HYDRUS-1D to simulate the transport of soil water isotopes with evaporation fractionation

Tiantian Zhou, Jirka Šimůnek, Isabelle Braud

Publisher: Elsevier

Journal: Environmental Modelling & Software

DOI: 10.1016/j.envsoft.2021.105118

Adapting HYDRUS-1D to Simulate the Transport of Soil Water Isotopes with Evaporation Fractionation

Tiantian Zhou[1,*], Jirka Šimůnek[1], and Isabelle Braud[2]

Corresponding author: email: tzhou035@ucr.edu; Tel: +1 951 880-4432

[1] Department of Environmental Sciences, University of California Riverside, CA 92521, United States

[2] INRAE, Riverly, 5 Rue de la Doua, 69625 Villeurbanne, Cedex, France

Abstract: Ecohydrological processes are often evaluated by studying the fate of stable water isotopes. However, isotopic fractionation during evaporation is often ignored or simplified in current models, resulting in simulation errors that may be propagated into practical applications of stable isotope tracing. In this study, we adapted and tested the HYDRUS-1D model, a numerical model widely used to simulate variably-saturated water flow and solute transport in porous media, by including an option to simulate isotope fate and transport while accounting for evaporation fractionation. The numerical results obtained by the adapted model were in excellent agreement with existing analytical solutions. Additional plausibility tests and field evaluation further demonstrated the adapted model's accuracy. A simple particle tracking algorithm was also implemented to calculate soil water's transit times and further validate the modified model's results. Transit times calculated by the particle tracking module (PTM) were similar to those estimated by the isotope peak displacement method, validating the applicability of the PTM. The developed model represents a comprehensive tool to numerically investigate many important research problems involving isotope transport processes in the critical zone.

Keywords: Water stable isotopes; Isotope transport modeling; HYDRUS-1D; Evaporation fractionation; Water transit time; Particle tracking algorithm.

1 Introduction

Evaporation fractionation is characterized by the retainment of heavier isotopes in the liquid phase and the preferential affinity of lighter isotopes in the vapor phase (e.g., *Gonfiantini et al.*, 2018). Due to evaporation fractionation's unique characteristics, stable water isotopes (^{2}H and ^{18}O) are good indicators for studying many ecohydrological processes in the critical zone (*Gehrels et al.*, 1998; *Sprenger et al.*, 2016a), such as partitioning evapotranspiration (*Kool et al.*, 2014; *Xiao et al.*, 2018) and identifying the sources of crop water uptake (i.e., sourcing) (e.g., *Corneo et al.*, 2018; *Ma and Song*, 2016; *Wang et al.*, 2019) at the soil-vegetation-atmosphere interface. Models that can accurately simulate the transport and fractionation of isotopes are necessary to properly interpret isotopic data in the critical zone.

The concept of water transit or travel time (TT), defined as the time elapsed between water entering and leaving a reservoir, provides a useful insight into many ecohydrological issues, such as partitioning recharge and discharge sources, evaluating the role of mobile and immobile waters, and inferring temporal origins of root water uptake (e.g., *Allen et al.*, 2019; *Brinkmann et al.*, 2018; *McDonnell*, 2014; *Sprenger et al.*, 2016b). The traditional isotope-based method for estimating TTs is by inversely estimating lumped isotope transport parameters assuming time-invariant TT distributions (TTDs) (e.g., *Maloszewski et al.*, 2006; *Stumpp and Maloszewski*, 2010; *Timbe et al.*, 2014) or StorAge Selection (SAS) functions (*Rinaldo et al.*, 2015). However, the lumped models overgeneralize the isotope transport mechanisms. Some of them cannot truly describe the isotope transport or TTDs under transient conditions, while others can account for the time-variance of TTDs but can only describe the mixing and partitioning of isotopes (*Jury et al.*, 1986; *Sprenger et al.*, 2016a). Physics-based isotope transport models are needed to fully describe the spatio-

temporal evolution of isotope concentrations under field conditions (*Kim et al.*, 2016). Such flow and transport models usually rely on the Richards and convection-dispersion equations, respectively.

When evaporation fractionation can be neglected, one can simulate the fate and transport of isotopes in soils as standard solutes. For example, *Stumpp et al*. (2012) used the modified HYDRUS-1D model with isotopic information to analyze the effects of the vegetation cover and fertilization measures on water flow and solute transport in lysimeters. This modified model is available at https://www.pc-progress.com/en/Default.aspx?h1d-lib-isotope. *Sprenger et al.* (2016b) used this modified model to infer soil water residence times at different depths. *Brinkmann et al.* (2018) applied the same model to estimate the residence time distribution of soil water and identify the temporal origin of water taken up by *Picea abies* and *Fagus sylvatica*.

This modified version of the HYDRUS-1D model by *Stumpp et al.* (2012) allows isotopes to leave the soil profile at the soil surface without considering the fractionation effect during evaporation. This is implemented by assuming that the isotope concentration of the evaporation flux is the same as that of soil water at the soil surface. However, ignoring the evaporative enrichment, as done in this modified HYDRUS-1D, leads to underestimating ^{2}H and ^{18}O concentrations in the topsoil, which may be more significant in regions with higher evaporative losses (*Sprenger et al.*, 2018). Additionally, transit times calculations as done in these studies (e.g., *Sprenger et al.*, 2016b; *Brinkmann et al.*, 2018) are based on isotope transport simulations and require labor-intensive and time-consuming high precision isotope measurements to calibrate the model. The inaccurate sampling or modeling of soil water isotopes, especially in case of physical-nonequilibrium (i.e., immobile water content, dual-porosity/permeability type solute transport), can easily lead to large errors in transit time calculations (e.g., *Sprenger et al.*, 2018; *Tetzlaff et al.*, 2014).

The temporal evolution of evaporation fractionation was first studied and modeled for the free water surface (*Craig and Gordon*, 1965). The Craig-Gordon model has been the cornerstone

of isotope hydrology since it was proposed in 1965. After that, *Zimmermann et al.* (1967) applied this model to saturated soil under steady-state evaporation conditions. *Barnes and Allison* (1983) extended this work to isothermal steady-state evaporation conditions in unsaturated soils. *Barnes and Allison* (1984) further extended this work to the nonisothermal steady-state conditions in unsaturated soils with a defined soil temperature profile. *Barnes and Allison* (1983, 1984) also provided analytical solutions for the transport of isotopes with evaporation fractionation under steady-state conditions. However, to describe and predict the spatial and temporal evolution of isotope concentrations under field evaporation conditions, a model capable of describing transient conditions is required.

Shurbaji and Phillips (1995) proposed the first numerical model (ODWISH) that considered evaporation fractionation. This model coupled heat transport and water flow equations in the soil proposed by *Philip and De Vries* (1957) and introduced a transition factor into the isotope transport equation. This transition factor combines the influence of hydrology and isotope parameters. It changes slowly with depth except for quick changes in the evaporative zone, which is conducive to obtaining a unique isotope profile shape. However, the upper boundary condition must be determined by measuring temperatures and humidities at the soil surface and the evaporation front. The evaporation front is located at a depth above which the water vapor flux becomes dominant compared to the liquid flux. Generally, it corresponds to the peak in the isotope concentration profile (*Braud et al.*, 2005a). Since such data are rarely available, a model that interacts with the atmosphere is needed to address the surface energy budget. *Mathieu and Bariac* (1996) proposed a simplified model (MOISE) for constant potential evaporation and a predefined soil temperature profile. This model still lacked the option of evaluating the surface energy budget (*Soderberg et al.*, 2013).

Melayah et al. (1996a) fully coupled the transport of heat, water, and isotopes with surface energy budget calculations. The results showed that the model was very sensitive to the initial isotope profile and small changes in liquid water convective transport. Better knowledge of isotope

transport coefficients in porous media (e.g., mobile/immobile phases) should improve its prediction ability (*Melayah et al.*, 1996b). *Braud et al.* (2005a) corrected some inconsistencies in the derivations of *Melayah et al.* (1996a) and several isotope transport models, such as SiSPAT-Isotope (*Braud et al.*, 2005a) and Soil-Litter-Iso (*Haverd and Cuntz*, 2010) have been developed based on this modified theory. The Soil-Litter-Iso model was based on Ross' explicit numerical solution of the Richards equation (*Ross*, 2003), resulting in significantly improved computational efficiency compared with the SiSPAT-Isotope model. This allowed isotope calculations to be performed for soil profiles with vegetation using coarser spatial discretization and larger time steps (*Haverd and Cuntz*, 2010). However, these models did not consider the impacts of physical nonequilibrium flow (e.g., immobile water or preferential flow) on isotope transport and concentrations. *Muller et al.* (2014) and *Sprenger et al.* (2018) used the SWIS model (Soil Water Isotope Simulator) to model stable isotopes for uniform and nonequilibrium (mobile and bulk) soil water flow in the vadose zone, respectively. This model considered evaporation fractionation but neglected vapor flow.

Despite the successes of isotope transport modeling with evaporation fractionation, the current isotope transport models (Table 1) are not widely used. Some of them are no longer maintained (e.g., *Mathieu and Bariac*, 1996; *Melayah et al.*, 1996), are quite complex to deploy (e.g., *Braud et al.*, 2005a; *Haverd and Cuntz*, 2010), or still only implement a simple treatment of evaporation fractionation (e.g., *Shurbaji and Phillips*, 1995; *Stumpp et al.*, 2012), which may be some of the reasons why they are not commonly used.

The standard version of HYDRUS-1D can simulate volatile solutes' transport in soils by allowing solute transport by convection and dispersion in the liquid phase and diffusion in the soil air. Thus, the model is quite widely used to simulate transport processes of many emerging organic chemicals such as pesticides and fumigants (e.g., *Spurlock et al*., 2013ab; *Brown et al*., 2019). The governing equations for volatile solute transport (see Eqs. (6.55) and (6.56) in *Radcliffe and Šimůnek*, 2018) are similar to those for the isotope transport by *Braud et al.* (2005a). The

relationship between the liquid and vapor solute concentrations is described in HYDRUS-1D by Henry's law, assuming an instantaneous distribution of a solute between the liquid and air phases. This volatile solute transport model in HYDRUS-1D can be adapted to simulate the transport of stable isotopes by modifying the upper boundary condition (considering fractionation) and reinterpreting Henry's coefficient in the governing solute transport equation.

Particle tracking algorithms represent an alternative and more straightforward way of calculating TTDs (e.g., *Šimůnek*, 1991; *Asadollahi et al.*, 2020) while still considering transient water flow. Since the particle tracking algorithm (e.g., *Šimůnek*, 1991) can be technically based solely on water balance calculations without requiring isotopic measurements, it needs much less input information than the stable water isotope transport models. Such algorithms can thus have broad applicability and can act as an excellent supplement to the traditional isotope transport-based methods for calculating transit times. However, it is still highly recommended to observe isotopic data, identifying accurate model parameters and travel times (e.g., *Groh et al.*, 2018; *Mattei et al.*, 2020; *Sprenger et al.*, 2015), and verifying model-determined TTs.

The objectives of this study thus are: 1) to adapt the current HYDRUS-1D model to simulate water flow and transport of stable water isotopes while considering multiple types of evaporation fractionation situations and soil conditions (i.e., isothermal/non-isothermal conditions, equilibrium and nonequilibrium flow, with and without vapor flow), 2) to verify the new model using analytical solutions and plausibility tests, 3) to implement a simple water-flow based particle tracking algorithm, and 4) to evaluate the capability of the new isotope transport and particle tracking modules using a field dataset. The new isotope transport and particle tracking modules provide HYDRUS-1D users with a comprehensive tool for assessing transit times, simulating continuous dynamic changes in soil water isotope concentrations, and numerically investigating many fundamental research problems involving sourcing and timing of soil water.

Table 1. History of the development of physics-based transport models for soil water stable isotopes.

Model name	Reference	Description
HYDRUS isotope module	*Stumpp et al.* (2012)	Without fractionation
ODWISH	*Shurbaji and Phillips* (1995)	With fractionation, no surface energy budget
MOISE	*Mathieu and Bariac* (1996); *Melayah et al.* (1996)	With fractionation, no surface energy budget
SiSPAT-Isotope	*Braud et al.* (2005a, 2005b)	With fractionation and surface energy budget, but no physical nonequilibrium flow, numerically inefficient
Soil-Litter-Iso	*Haverd et al.* (2010)	With fractionation and surface energy budget, but no physical nonequilibrium flow
SWIS	*Muller et al.* (2014); *Sprenger et al.* (2018)	With fractionation but without vapor flow

2 Definition of the isotope concentrations

Following *Braud et al.* (2005a), the concentration C_i (kg m^{-3}) of the isotope *i*, can be defined as:

$$C_i = \frac{m_i}{V} = \frac{m_i}{m_T}\frac{m_T}{V} = \frac{N_i M_i}{N_i M_i + N_w M_w}\frac{N_i M_i + N_w M_w}{V} \approx \frac{M_i}{M_w} R_i \rho \qquad (1)$$

where m_i (kg) is the mass of the isotope *i*, either in the liquid or vapor phase, V (m^3) is the volume of water, m_T (kg) is the total mass of water, M_i and M_w are the molar masses of water including the isotope *i* and ordinary water (kg/mol), respectively, N_i and N_w (mol) are the numbers of moles of water including the isotope *i* and ordinary water, respectively, R_i [-] is the isotope ratio of the isotope *i* (i.e., $\frac{N_i}{N_w}$), and ρ (kg/m^3) is the density of water either in the liquid (ρ_w) or vapor (ρ_v) phases (see Appendix A). In this equation, we assumed that $N_i M_i \ll N_w M_w$ to get the last term.

The relationship between the isotope ratio R and isotopic composition δ is:

$$\delta_i(‰) = \frac{R_i - R_{\text{std}}}{R_{std}} 1000‰ \quad (2)$$

where R_i and $R_{standard}$ are the isotope ratios in the water sample and the standard sample (the Vienna Standard Mean Ocean Water (VSMOW, 0‰), $R_{std} = 155.76 \times 10^{-6}$ for HDO and $R_{standard} = 2005.2 \times 10^{-6}$ for $H_2{}^{18}O$, according to *Gonfiantini* (1978)). R_i refers to the $^{18}O/^{16}O$ or $^{2}H/^{1}H$ ratios [-] that can be deduced from Eq. (1) as follows:

$$R_i = \frac{M_w}{M_i} \frac{C_i}{\rho} \quad (3)$$

Note that in this study, the term isotope ratio refers to R [-], isotopic composition refers to δ (‰), and isotope concentration to C (kg m^{-3}). The results will be presented throughout the manuscript in δ-notation, even though numerical computations may be performed using the C, R, or δ notations.

3 Craig-Gordon model (1965)

The separation of heavy and light isotopes between reservoirs (or reactants and products) is called isotopic fractionation (*Gat*, 2010; *Kendall and McDonnell*, 2012). Isotopic fractionation can be divided into equilibrium fractionation (chemical thermodynamic fractionation) and kinetic fractionation (physical diffusion fractionation) according to the processes that cause this change. Equilibrium fractionation occurs during chemical reactions at equilibrium (exchange reactions); the heavy isotopes are concentrated in substances with the highest bond force constants (i.e., the preferential affinity of the lighter isotope for the vapor phase) (*Fry*, 2006). Kinetic fractionation is caused by the differences in the diffusion rates of water molecules through the air (i.e., preferential diffusion of the lighter isotope) (*Gat*, 2010). Evaporation fractionation between the soil and free atmosphere includes both equilibrium and kinetic fractionations (*Craig*, 1961). *Craig and Gordon* (1965) calculated the isotope evaporation flux at the liquid-vapor interface based on these two types of fractionations.

This model considers three layers (Fig. 1): (a) a liquid-vapor interface where condensation, evaporation, and equilibrium fractionation occur, (b) a diffusive sublayer where molecular

diffusion dominates and thus kinetic fractionation occurs, and (c) a turbulently mixed sublayer where mixing dominates, and thus no fractionation occurs (*Gat*, 2010; *Horita et al.*, 2008). The water vapor and isotope evaporation fluxes between the water surface and the bottom of the free atmosphere are described by Ohm's Law (or Fick's law) as an analog of the concentration gradient and transport resistance (*Braud et al.*, 2005a; *Braud et al.*, 2009; *Gat*, 2010).

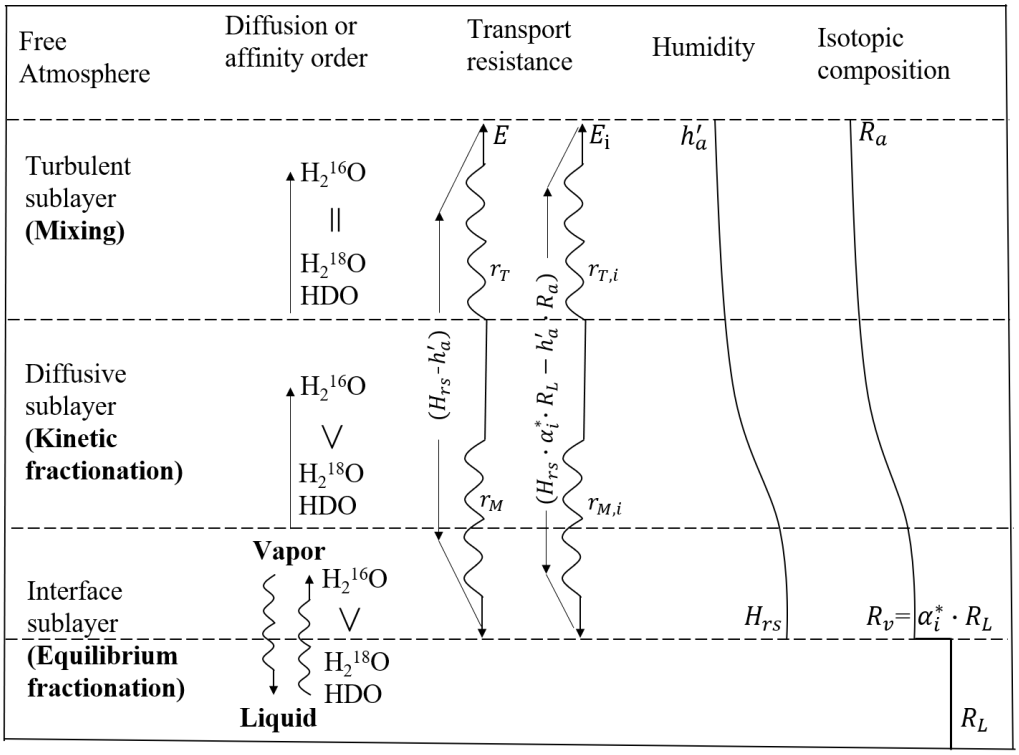

Figure 1. The Craig–Gordon model of isotopic fractionation during evaporation (modified from *Gat*, 2010).

The evaporation flux for water vapor E (kg/m^2/s) is:

$$E = \frac{\rho_{sat}^{v}(T_s)(H_{rs} - h_a')}{r_a} \quad (4)$$

where r_a (s/m) is the sum of the resistances (r_M+r_T) of water vapor to diffusive flow in the diffusive (r_M) and turbulent (r_T) sublayers, ρ_{sat}^{v} is the density of the saturated water vapor (kg/m^3) (see Appendix A), H_{rs} [-] is the relative humidity of the soil air phase at the surface, and h_a' [-]

is the relative humidity of the atmosphere at the air temperature T_a (K) normalized to the relative humidity of the atmosphere (h_a [-]) at the interface temperature T_s (K). H_{rs} and h_a' can be calculated as follows:

$$H_{rs} = exp(\frac{Mgh_s}{R_u T_s}) \tag{5}$$

$$h_a' = h_a \frac{\rho_{sat}^v(T_a)}{\rho_{sat}^v(T_s)} \tag{6}$$

where g is the gravitational acceleration [LT^{-2}], M is the molecular weight of water (kg/mol) (0.018015), R_u is the universal gas constant (J/mol/K) (8.314), h_s is the matric potential at the soil surface [L], and T_s and T_a are the temperatures of the soil surface and atmosphere (K), respectively.

The corresponding evaporation flux for water isotopes E_i (kg/m^2/s) is:

$$\begin{aligned} E_i &= \frac{(C_{is}^v - C_{ia}^v)}{r_i} = \frac{(C_{is}^v - C_{ia}^v)}{\alpha_i^k \cdot r_a} = \frac{\rho_{sat}^v(T_s)}{\alpha_i^k r_a}\frac{M_i}{M_w}(H_{rs}\cdot\alpha_i^*\cdot R_L - h_a'\cdot R_a) \\ &= \frac{E}{\alpha_i^k}\frac{M_i}{M_w}\frac{(H_{rs}\cdot\alpha_i^*\cdot R_L - h_a'\cdot R_a)}{H_{rs}-h_a'} \end{aligned} \tag{7}$$

The isotope ratio of the evaporation flux R_E is:

$$R_E = E_i/E = [H_{rs}\cdot\alpha_i^*\cdot R_L - h_a'\cdot R_a]/[(H_{rs}-h_a')\cdot\alpha_i^k]\cdot\frac{M_i}{M_w} \tag{8}$$

where C_{is}^v and C_{ia}^v are the isotope concentrations of the surface water vapor and atmosphere (kg m^{-3}), r_i (s/m) is the sum of the resistances (r_{Mi}+r_{Ti}) of water isotopes to diffusive flow in the diffusive (r_{Mi}) and turbulent (r_{Ti}) sublayers, $R_v(R_L)$ are the isotope ratios of the water vapor and remaining liquid water at the soil surface [-], respectively, R_a is the isotope ratio of the atmosphere [-], α_i^* is the equilibrium fractionation factor [-], and α_i^k is the kinetic fractionation factor [-]. Note that α_i^* is defined here as the ratio of vapor to liquid phase isotope ratios, and it is thus smaller than 1.

The equations used to compute α_i^* for ^{2}H and ^{18}O isotopes as a function of temperature T (K) can be found in *Majoube* (1971) and *Horita and Wesolowski* (1994). The equations by *Majoube* (1971) were used in this study:

$$\alpha_i^*\left(\frac{^{18}O}{^{16}O}\right) = \exp(2.0667 \cdot 10^{-3} + \frac{0.4156}{T} - \frac{1.137 \cdot 10^3}{T^2}) \quad (9)$$

$$\alpha_i^*\left(\frac{^{2}H}{^{1}H}\right) = \exp(-52.612 \cdot 10^{-3} + \frac{76.248}{T} - \frac{24.844 \cdot 10^3}{T^2}) \quad (10)$$

The kinetic fractionation factor α_i^k is calculated as (*Mathieu and Bariac*, 1996):

$$\alpha_i^k = \left(\frac{D^v}{D_i^v}\right)^{n_k} \quad (11)$$

where n_k is the kinetic fractionation coefficient [-], and D^v and D_i^v are the molecular diffusion coefficients of light and heavy water (isotopes) in free air [L^2T^{-1}], respectively.

The diffusion ratio D^v/D_i^v can be calculated from Graham's Law of gas diffusion:

$$\frac{D^v}{D_i^v} = \left(\frac{M_i(M_w + 0.029)}{M_w(M_i + 0.029)}\right)^{1/2} \quad (12)$$

where the number 0.029 represents the mean molecular weight of air (kg/mol). For ^{18}O, M_w=0.018 kg/mol and M_i=0.020 kg/mol, and thus D^v/D_i^v=1.0324; while for ^{2}H, M_w=0.018 kg/mol and M_i=0.019 kg/mol, and thus D^v/D_i^v=1.0166, which are the values used in our study. In addition to these theoretical values, much research has been conducted to measure these values. Readers are referred to *Horita et al.* (2008) for more details. For example, *Merlivat* (1978) measured $D^v/D_i^v(^2H)$=1.0251 and $D^v/D_i^v(^{18}O)$=1.0285.

The kinetic fractionation coefficient n_k is associated with considerable uncertainty depending on evaporation conditions. Different equations have been used to calculate this value. Readers can refer to *Braud et al.* (2005b), *Horita et al.* (2008), and *Quade et al.* (2018) for more details. Table S1 shows the equations used in this study.

The equilibrium fractionation enrichment ε^* (‰), and the kinetic fractionation enrichment ε_k (‰) can be calculated as follows (*Gat*, 2010):

$$\varepsilon^* = 1000 \cdot (1 - \alpha_i^*) \quad (13)$$

$$\varepsilon_k = 1000 \cdot \left(\alpha_i^k - 1\right) \cdot (H_{rs} - h_a{}') \quad (14)$$

This equation can be further simplified to get the widely used kinetic fractionation enrichment equation (*Horita et al.*, 2008):

$$\varepsilon_k = 1000 \cdot \left(\left(\frac{D^v}{D_i^v}\right)^{n_k} - 1\right) \cdot (H_{rs} - h_a') \cong 1000 \cdot n_k \cdot \left(\frac{D^v}{D_i^v} - 1\right) \cdot (H_{rs} - h_a') \quad (15)$$

According to *Gonfiantini* (1986), the total fractionation factor (α_i^{total}) can be simplified and expressed as follows:

$$\alpha_i^{total} = 1/\alpha_i^* + \frac{\varepsilon_k}{1000} \quad (16)$$

The isotope ratio of the evaporation flux (R_E) is then calculated using its linear relationship with the isotope ratio of the liquid phase (R_L):

$$R_E = R_L/\alpha_i^{total} \quad (17)$$

4 Numerical models

The current isotope transport models can be generally divided into two groups. The first group includes numerical models for evaporation fractionation without vapor flow. These models can be used in relatively humid areas, where the evaporation front is close to the ground surface, and vapor flow in the soil profile can thus be neglected. There is no fractionation within the soil due to the lack of the vapor phase (or its consideration). The second group includes numerical models for evaporation fractionation with vapor flow. These models are intended for more arid zones, where the evaporation front can occur deeper in the soil profile, and vapor flow in the soil profile should thus be considered. Under such conditions, both equilibrium and kinetic fractionations must be considered within the soils (*Braud et al.*, 2005a; *Mathieu and Bariac*, 1996). For the calculation of relevant water flow and heat transport parameters, the readers are referred to the HYDRUS-1D manual (*Šimůnek et al.*, 2008). Here we only focus on the calculation of isotope-related parameters.

4.1 Evaporation fractionation in a system that neglects vapor flow

When vapor flow can be neglected (e.g., in humid zones), the one-dimensional uniform soil water movement in HYDRUS-1D can be described using the Richards equation, which assumes that the air phase plays a negligible role in water flow and water flow due to thermal gradients can be neglected (*Šimůnek et al.*, 2008). The governing equation for water flow then is:

$$\frac{\partial \theta_l}{\partial t} = \frac{\partial}{\partial z}\left[K_{Lh}\left(\frac{\partial h}{\partial z} + cos\gamma\right)\right] - S \tag{18}$$

where θ_l is the liquid volumetric water content [L^3L^{-3}], t is time [T], h is the water pressure head [L], z is the spatial coordinate [L] (positive upward), γ is the angle between the flow direction and the vertical axis, K_{Lh} is the isothermal hydraulic conductivity of the liquid phase [LT^{-1}], and S is the sink term [$L^3L^{-3}\ T^{-1}$].

Since there is no fractionation within the soil, the governing equation for the isotope transport is the same as the classical advection-dispersion equation:

$$\frac{\partial \theta_l C_i^l}{\partial t} = \frac{\partial}{\partial z}(D_i^{l*}\frac{\partial C_i^l}{\partial z}) - \frac{\partial (q_l C_i^l)}{\partial z} - SC_i^l \tag{19}$$

where C_i^l corresponds to isotope concentrations of soil water (kg m^{-3}), q_l is the liquid water flux [LT^{-1}], and D_i^{l*} is the effective dispersion coefficient of the isotope i in soil water [L^2T^{-1}]. Evaporation fractionation, which does not appear in Eq (19), is considered using the upper boundary condition. Since Eq. (19) is a linear equation, linear conversions of concentration do not affect the numerical results. Therefore, not only the C notation, but also the R or δ notations can be used to define isotope concentrations in the numerical model.

Compared with traditional solute transport models, which leave all solutes behind in the soil during evaporation, the isotope transport models allow isotopes to leave with evaporation. *Stumpp et al.* (2012) did not consider fractionation and assumed that the isotope concentration of the evaporation flux is the same as that of the soil water at the soil surface. Here, the isotope ratio of the evaporation flux is instead evaluated using two methods. The first method uses the Craig-Gordon model (Eq. (8)), which requires the atmosphere's relative humidity, temperature, and

isotope ratio as additional inputs. The second approach follows the *Gonfiantini* (1986) model (Eqs 16~17), which requires only the atmosphere's relative humidity as an additional input. The isotope ratio of the evaporation flux is then automatically used in HYDRUS to calculate the isotope evaporation flux at the upper boundary corresponding to the water flux.

4.2 Evaporation fractionation in a system that considers vapor flow

a. Water flow

Vapor flow in the soil profile should be considered in many arid zones. Nonisothermal liquid and vapor flow in HYDRUS-1D is described as follows (*Saito et al.*, 2006; *Zheng et al.*, 2020):

$$\frac{\partial \theta_T(h)}{\partial t} = \frac{\partial}{\partial z}\left[K_{Lh}\left(\frac{\partial h}{\partial z} + cos\gamma\right) + K_{LT}\frac{\partial T}{\partial z} + K_{vh}\frac{\partial h}{\partial z} + K_{vT}\frac{\partial T}{\partial z}\right] - S \quad (20)$$

$$q_l = -K_{Lh}\left(\frac{\partial h}{\partial z} + cos\gamma\right) - K_{LT}\frac{\partial T}{\partial z} \quad (21)$$

$$q_v = -K_{vh}\frac{\partial h}{\partial z} - K_{vT}\frac{\partial T}{\partial z} \quad (22)$$

where θ_T is the total volumetric water content [L^3L^{-3}], being the sum ($\theta_T = \theta_l + \theta_v$) of the volumetric liquid water content (θ_l) and the volumetric water vapor content (θ_v) [L^3L^{-3}] (both expressed in terms of equivalent water contents, i.e., $\theta_v = \rho_v \frac{\theta_s - \theta_l}{\rho_w}$, where θ_s is the saturated water content [L^3L^{-3}]), K_{LT} is the thermal hydraulic conductivity of the liquid phase [$L^2K^{-1}T^{-1}$], K_{vh} is the isothermal vapor hydraulic conductivity [LT^{-1}], K_{vT} is the thermal vapor hydraulic conductivity [$L^2K^{-1}T^{-1}$], and q_v is the vapor flux [LT^{-1}]. The right-hand side of Eq. (20) represents isothermal liquid flow, gravitational liquid flow, thermal liquid flow, isothermal vapor flow, and thermal vapor flow, respectively. Since several terms are a function of temperature, this equation should be solved simultaneously with the heat transport equation to account for temporal and spatial changes in soil temperature properly.

b. Heat transport

The governing equation for heat transport is (*Šimůnek et al.*, 2008):

$$C_p(\theta_l)\frac{\partial T}{\partial t} + L_0\frac{\partial \theta_v}{\partial t} = \frac{\partial}{\partial z}\left(\lambda(\theta_l)\frac{\partial T}{\partial z}\right) - C_w q_l \frac{\partial T}{\partial z} - C_v \frac{\partial q_v T}{\partial z} - L_0\frac{\partial q_v}{\partial z} - C_w S T \quad (23)$$

where $\lambda(\theta_l)$ is the coefficient of the apparent thermal conductivity of the soil [$MLT^{-3}K^{-1}$] and $C_p(\theta_l)$, C_w, and C_v are the volumetric heat capacities [$ML^{-1}T^{-2}K^{-1}$] of the porous medium, the liquid phase, and vapor phase, respectively. L_0 is the volumetric latent heat of vaporization of liquid water [$ML^{-1}T^{-2}$]. The right-hand side of Eq. (23) represents the conduction of sensible heat (the first term), convection of sensible heat by liquid water (the second term) and water vapor (the third term), and convection of latent heat by vapor flow (the fourth term), and energy uptake by plant roots (the fifth term), respectively.

c. Isotope transport

Following the theory of the SiSPAT-Isotope model (*Braud et al.*, 2005a), the total isotope flux is the sum of isotope fluxes in the liquid phase, q_i^l, and the vapor phase, q_i^v, while both fluxes include convection and diffusion terms. Assuming instantaneous equilibrium between the liquid and vapor phases, the liquid and vapor isotopic ratios can be related by an equilibrium fractionation factor (*Mathieu and Bariac*, 1996; *Melayah et al.*, 1996a). The governing equations for isotope transport then are:

$$\frac{\partial\{[\theta_l + (n_{soil} - \theta_l)\beta_i^*]C_i^l\}}{\partial t} = -\frac{\partial}{\partial z}\left[q_i^l + q_i^v\right] - SC_i^l \quad (24)$$

$$\frac{\partial\{[\theta_l + (n_{soil} - \theta_l)\beta_i^*]C_i^l\}}{\partial t} = -\frac{\partial}{\partial z}[C_i^l q_l - D_i^{l*}\frac{\partial C_i^l}{\partial z} + \beta_i^* q_v C_i^l - D_i^{v*}\frac{\partial \beta_i^* C_i^l}{\partial z}] - SC_i^l \quad (25)$$

$$\frac{\partial\{[\theta_l + (n_{soil} - \theta_l)\beta_i^*]C_i^l\}}{\partial t} = -\frac{\partial}{\partial z}[(q_l + \beta_i^* q_v - D_i^{v*}\frac{\partial \beta_i^*}{\partial z})C_i^l - (D_i^{l*} + D_i^{v*}\beta_i^*)\frac{\partial C_i^l}{\partial z}] - SC_i^l \quad (26)$$

that is:

$$\frac{\partial[\Theta_i C_i^l]}{\partial t} = \frac{\partial}{\partial z}[D_i^{lv*}\frac{\partial C_i^l}{\partial z} - Q_i^{lv*}C_i^l] - SC_i^l \quad (27)$$

$$\Theta_i = [\theta_l + (n_{soil} - \theta_l)\beta_i^*] \quad (28)$$

$$Q_i^{lv*} = (q_l + \beta_i^* q_v - D_i^{v*}\frac{\partial \beta_i^*}{\partial z}) \quad (29)$$

$$D_i^{lv*} = D_i^{l*} + D_i^{v*}\beta_i^* \quad (30)$$

$$C_i^v = \beta_i^* C_i^l \quad (31)$$

$$C_i^v = \frac{M_i}{M_w}R_i^v\rho_v = \frac{M_i}{M_w}\alpha_i^* R_i^l \rho_v = \alpha_i^*\frac{\rho_v}{\rho_w}C_i^l \quad (32)$$

where n_{soil} is the soil porosity [L^3L^{-3}], β_i^* is the ratio of the isotope concentration in the vapor phase and the isotope concentration in the liquid phase [-], and C_i^l (R_i^l) and C_i^v (R_i^v) are isotope concentrations (ratios) in soil water (vapor) (kg m^{-3}) ([-]), respectively. The effective dispersion coefficients of the isotope *i* in soil water (vapor), D_i^{l*} (D_i^{v*}) [L^2T^{-1}], are given as follows:

$$D_i^{l*} = D_i^{lo}\tau_w\theta_l + \Lambda|q_l| \quad (33)$$

$$D_i^{v*} = (n_{soil} - \theta_l)\tau_g D^v(\frac{D_i^v}{D^v})^{n_k} \quad (34)$$

where τ_w and τ_g are tortuosity coefficients in the liquid and vapor phases [-], respectively, Λ is dispersivity [L], and D_i^{lo} is the molecular diffusion coefficient of the isotope *i* in free water [L^2T^{-1}] (see Appendix A).

d. Modifications on HYDRUS-1D

This subsection lists all implemented changes into the standard HYDRUS-1D model to simulate the fate and transport of stable water isotopes. To expand the capabilities of the HYDRUS-1D model and to be consistent with previous verification studies with other models (e.g., the plausibility tests and comparisons with the analytical solution of *Barnes and Alison*, 1984), a new upper boundary condition (BC) for water flow was implemented into the atmospheric boundary in HYDRUS-1D to simulate evaporation from bare soils. Actual evaporation E (kg/m^2/s) is calculated in this BC as a function of potential evaporation E_p (kg/m^2/s) and the difference in relative humidities between the atmosphere and the soil surface, similarly as done in other studies (*Mathieu and Bariac*, 1996; *Melayah et al*., 1996; *Braud et al*., 2005a). This is a more

convenient way of estimating actual evaporation at the upper boundary. However, if sufficient information is available, it is better to use the surface energy balance to estimate actual evaporation.

$$E = E_p \frac{H_{rs} - h_a{}'}{1 - h_a{}'} \tag{35}$$

The standard version of HYDRUS-1D can simulate the transport of volatile solutes by also considering solute transport via diffusion in the vapor phase. The governing equations for volatile solute transport (see Eqs. (6.55) and (6.56) in *Radcliffe and Šimůnek*, 2018) are very similar to those for isotope transport. The solute transport equation solved in HYDRUS-1D considers convective and diffusion-dispersion transport in the liquid phase and diffusion transport in the vapor phase. It does not consider convective transport in the vapor phase. To consider the vapor convection term in solute transport, two additional transport terms ($\beta_i^* q_v$) and ($D_i^{v*} \frac{\partial \beta_i^*}{\partial z}$) in Eq. (29) had to be included in the governing solute transport equation of HYDRUS-1D.

HYDRUS-1D considers the relationship between the liquid and vapor solute concentration that assumes instantaneous linear distribution of a solute between the liquid and vapor phases (Henry's law):

$$C_i^v = K_H C_i^l \tag{36}$$

where K_H is the Henry coefficient [-], which can be temperature-dependent. HYDRUS-1D assumes that temperature dependency can be expressed using the Arrhenius equation. To model the isotope transport using the current volatile solute boundary condition in HYDRUS, one can replace the original Henry coefficient (K_H) with the ratio of the isotope concentration in the vapor phase and the isotope concentration in the liquid phase ($\beta_i^* = \frac{\rho_v}{\rho_w} \alpha_i^*$). Since the density of water vapor ρ_v is a function of relative humidity of soil air phase (i.e., the soil matric potential), while equilibrium fractionation factor α_i^* is a function of soil temperature, the Henry coefficient for isotope transport is, in general, a function of both depth z and temperature T.

The standard HYDRUS-1D uses the stagnant boundary layer BC for volatile solutes. This BC considers the convective solute flux with evaporation and the diffusion solute flux (by gaseous

diffusion) through a stagnant boundary layer on the soil surface (*Jury et al.*, 1983). This upper boundary condition was modified to implement the Craig-Gordon model to account for both equilibrium and kinetic fractionations at the interface between the soil surface and the atmosphere (Eq. (7)).

4.3 The particle tracking module (PTM)

To calculate soil water travel times, the particle tracking algorithm from *Šimůnek* (1991) was implemented into HYDRUS-1D. The algorithm is based on the water balance calculations, with the development of soil water profiles fully described by solving the Richards equation (Fig. 2).

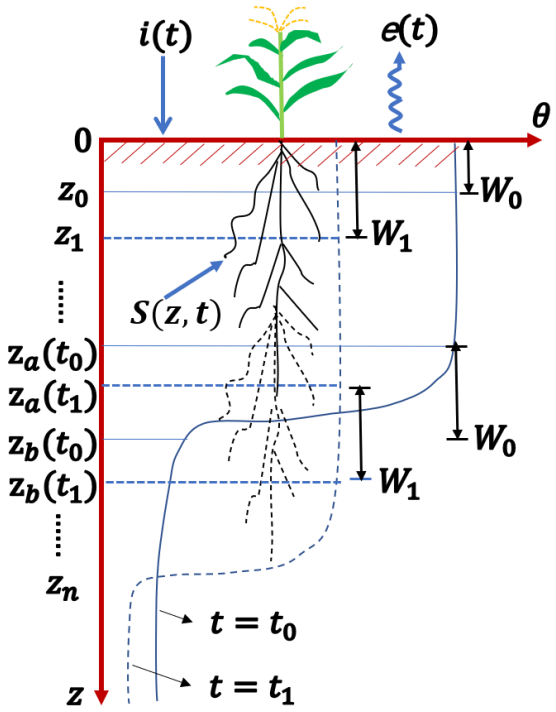

Figure 2. Schematic diagram of the water flow-based particle tracking module.

The first monitored particle below the soil surface is at depth $z = z_0$ at time $t = t_0$. The amount of water W_0 [L] is between this particle and the soil surface ($z = 0$):

$$W_0 = \int_0^{z_0} \theta(z, t_0) dz \tag{37}$$

During the time interval (t_0, t_1), the amount of water N [L] passes through the soil surface:

$$N = \int_{t_0}^{t_1} [e(t) - i(t)]dt \tag{38}$$

where $e(t)$ [LT^{-1}] is actual evaporation and $i(t)$ [LT^{-1}] is actual infiltration from precipitation or irrigation. During the same interval, the layers in the root zone between the soil surface and the monitored particles are depleted by root water uptake S_T [L]:

$$S_T = \int_{t_0}^{t_1} \int_{0}^{z_p(t)} s(z,t)dzdt \tag{39}$$

where $z_p(t)$ is the particle depth at time t [L] and $s(z,t)$ is the sink (extraction) term [L^{3}L^{-3} T^{-1}]. At time t_1, there is thus between the soil surface and the monitored particle the following quantity of water W_1 [L] (enriched by infiltration and reduced by evaporation and root water uptake):

$$W_1 = W_0 - N - S_T \tag{40}$$

The monitored particle is now located at a depth of $z = z_1$.

$$\int_0^{z_1} \theta(z,t_1)dz = \int_0^{z_0} \theta(z,t_0)dz - \int_{t_0}^{t_1} [e(t) - i(t)]dt - \int_{t_0}^{t_1} \int_0^{z_p(t)} s(z,t)dzdt \tag{41}$$

By repeatedly solving this equation for the time sequence (t_0, t_1, …, t_n), we obtain a sequence of depths (z_0, z_1, …, z_n), i.e., we obtain the trajectory of the observed particle.

The calculation of the location of the second and further particles can be performed analogously. Now, however, the amount of water is balanced between the next two particles located at z_a and z_b. Between these particles, the amount of water W_0, at time t_0 and the amount of water W_1 at time t_1 are:

$$W_0 = \int_{z_{a(t_0)}}^{z_{b(t_0)}} \theta(z,t_0)dz \tag{42}$$

$$W_1 = \int_{z_{a(t_1)}}^{z_{b(t_1)}} \theta(z, t_1) dz \tag{43}$$

During the time interval (t_0, t_1), the amount of water between the two particles is depleted by the transpiration amount S_T:

$$S_T = \int_{t_0}^{t_1} \int_{z_a(t)}^{z_b(t)} s(z, t) dz dt \tag{44}$$

According to Eq. (40), the resulting equation now has the form:

$$\int_{z_{a(t_1)}}^{z_{b(t_1)}} \theta(z, t_1) dz = \int_{z_{a(t_0)}}^{z_{b(t_0)}} \theta(z, t_0) dz - \int_{t_0}^{t_1} \int_{z_a(t)}^{z_b(t)} s(z, t) dz dt \tag{45}$$

The algorithm itself proceeds as follows. From the particles' known position at the beginning of the time interval, the pre-solved development of the moisture profile, and the actual values of infiltration, evaporation, and transpiration, the first monitored particle's new position is calculated using Eq. (41). New positions of all other particles are then calculated using Eq. (45). On the surface and at the bottom of the soil profile, new particles may be created or may leave the soil profile, depending on the moisture profile's actual development. By calculating particles' trajectories, the movement of inert substances not subject to dispersion can be modeled.

The initial position of particles can be defined geometrically (at specified depths) or based on mass balance calculations (by water storage). Similarly, the release of new particles at the boundary can be defined chronologically (at specified times) or meteorologically (rainfall events or depths). The newly implemented particle tracking module requires two input parameters: w_{Stand} and w_{Prec}. The w_{Stand} parameter represents the water storage, which separates neighboring particles in the soil profile at the beginning of the simulation. Therefore, the particles are not geometrically evenly distributed when the soil profile's initial water content is not uniform. The w_{Prec} parameter is the amount of water that passes through the soil surface before a new particle is released. This means that particles are released at the soil surface only under wet conditions. Under dry conditions, the surface flux is directed out of the soil profile, and thus, new particles will not be released.

5 Numerical implementations

The same graphical user interface (GUI) used in HYDRUS-1D is used to select and execute the model. The HYDRUS software uses the finite element method for spatial discretization and the finite difference method for temporal discretization. For consistency with the numerical model (the SiSPAT-Isotope model) used for the verification, the Galerkin-type finite element method (FEM) and an implicit finite difference scheme were used to solve the Richards and advection-dispersion equations for water flow and isotope transport in this study. However, the upstream weighting FEM for space weighting and the Crank-Nicholson scheme for time weighting are also available. At each time step, the isotope transport is calculated after the water flow and heat transport equations have been solved first. This provides the isotope transport routine with nodal values of soil temperature, soil matric potential, and water content at both old and new time levels to constitute the storage and transport coefficients for isotope transport in Eqs. (27)-(32). Details about the numerical solutions of subsurface water flow and heat and solute transport can be found in the HYDRUS-1D manual (*Šimůnek et al.*, 2008) and *Braud* (2000).

To adequately capture the isotope concentration at the soil surface, similar to the SiSPAT-Isotope model, the isotope transport equation's solution requires a fine resolution of the vertical unsaturated soil profile close to the soil surface. Three discretization schemes (i.e., coarse, medium, and fine) (Fig. S1) were selected in the following verification examples to explore the impact of spatial discretization on the modeling results. The first scheme uses 101 nodes uniformly distributed in the soil profile, i.e., with a spatial step of 1 cm. The second scheme uses 288 nodes with spatial steps gradually increasing from the bottom to the top, being twice as large at the bottom (0.46 cm) than the top (0.23 cm). The third scheme follows the same spatial discretization as used by *Braud et al.* (2005a) with 288 nodes (Fig. S1). The spatial steps increase from 1 μm at the surface to 1 mm at a depth of about 1 cm and 5 mm at 5 cm. They remain 5 mm between depths of about 5 to 95 cm and then gradually decrease to 1 mm at the bottom. Only the modeling results

obtained using the fine spatial discretization are presented in the main text. The results obtained using medium and coarse spatial discretizations can be found in the Supplementary Material.

While the initial time step of 25 s was used in this study, time steps vary during the simulation. They are automatically adjusted by the model depending on the number of iterations required by the water flow scheme to converge (adaptive time discretization). Since the adaptive time discretization was used, the temporal resolution is expected to have only a minor effect on the results and is not discussed in this study.

It must be emphasized that the accuracy of the numerical solution of isotope transport equations is very sensitive to those of water flow and heat transport equations. The water flow iteration process continues until absolute changes in water contents (pressure heads) at all nodes in the unsaturated (saturated) zone between two successive iterations are less than prescribed tolerances. We used 10^{-7} for both water content and pressure head (m) tolerances. When heat transport is also considered, water flow and heat transport equations are solved simultaneously since they affect each other. Two choices are provided in this case, depending on whether the nodal water flux balance smaller than a prescribed tolerance (10^{-16} m/s) is used as a convergence criterion for water flow and heat transport. The former iteration criterion without the nodal water flux balance is more numerical efficient and more applicable for systems that neglect vapor flow. The latter convergence criterion with the nodal water flux balance is more accurate and recommended for a system that considers vapor flow. Note that iterations are not needed in standard HYDRUS-1D for solute transport when the governing solute transport equation is linear. In this study, the difference in the isotope flux at the upper boundary between two successive iterations smaller than a prescribed tolerance (10^{-16} kg/m^2/s) was added as a convergence criterion for isotope transport. The above iterative criteria are important prerequisites for obtaining accurate numerical solutions. It is worth mentioning that the new HYDRUS isotope transport model is faster than the SiSPAT-Isotope model when no heat transport is considered because fewer iterations are required by the water flow scheme to converge.

6 Model verification and evaluation

6.1 Verification of the numerical solutions

First, we verified the numerical model that considers evaporation fractionation without vapor flow against the analytical solution of *Zimmermann et al.* (1967) for isothermal saturated soils under steady evaporation. Second, the numerical model that considers evaporation fractionation with vapor flow was then verified against the analytical solution of *Barnes and Allison* (1984) for nonisothermal unsaturated soils under steady evaporation. Third, *Mathieu and Bariac* (1996) designed six plausibility tests for isothermal unsaturated soils to check whether the model produces plausible results as equilibrium and kinetic fractionations were sequentially switched on in the model. *Braud et al.* (2005a) and *Haverd and Cuntz* (2010) used these tests to verify the SiSPAT-Isotope and Soil-Litter-Iso models, respectively. We repeated these tests with the HYDRUS-1D Isotope model to see whether the new model produced expected shapes of isotope profiles.

We considered a one-meter deep soil profile of Yolo Light Clay from *Philip* (1957) in all verification examples. Basic soil hydraulic, thermal, and solute transport parameters are given in *Braud et al.* (2005a) and shown in Table 2. For consistency with previous studies, we combined the van Genuchten (VG) water retention model (*van Genuchten*, 1980) with the *Burdine* (1953) and Brooks and Corey (BC) hydraulic conductivity model (*Brooks and Corey*, 1964):

$$\frac{\theta_l - \theta_r}{\theta_s - \theta_r} = \frac{1}{[1 + |\alpha h|^n]^m} \tag{46}$$

$$m = 1 - 2/n \tag{47}$$

$$K(\theta) = K_s(\frac{\theta_l - \theta_r}{\theta_s - \theta_r})^\eta \tag{48}$$

where θ_s and θ_r are saturated and residual water content, respectively, m, n, and α, are the shape parameters of the retention curve, K_s is the saturated hydraulic conductivity, and η is the shape parameter of the conductivity curve.

Equations from *de Vries* (1963) and *Chung and Horton* (1987) (already available in HYDRUS) were used to describe the volumetric heat capacity and thermal conductivity, respectively. The tortuosity coefficients in the liquid and vapor phases (τ_w and τ_g) are evaluated in HYDRUS using the model of *Millington and Quirk* (1991) or *Moldrup et al.* (1997). In all verification examples, τ_w and τ_g were set to 0.67, and Λ was set to 0 to be consistent with previous studies to evaluate our model's accuracy. This choice is justified because convective and hydrodynamic dispersion processes are negligible compared with the diffusion process under evaporation conditions (*Auriault and Adler*, 1995).

Table 2. Basic soil hydraulic, thermal, and solute transport parameters.

Parameter	**Symbol**	**Value**
Saturated water content	θ_s	0.35 m^3/m^3
Residual water content	θ_r	0.00 m^3/m^3
Shape parameter of the retention curve	n	2.22
Shape parameter of the retention curve	m	0.099
Shape parameter of the retention curve	α	5.18 m^{-1}
Saturated hydraulic conductivity	K_s	1.23×10^{-7} m/s
Shape parameter of the conductivity curve	η	9.143
Volumetric fraction of the solid phase	θ_n	0.60
Volumetric fraction of organic matter	θ_o	0.01
Empirical parameters	b_i (i=1,2,3)	-0.197, -0.962, 2.521 $Wm^{-1}K^{-1}$
Volumetric heat capacity of the solid phase	C_n	1920000 $Jm^{-3}K^{-1}$
Volumetric heat capacity of the organic matter	C_0	2510000 $Jm^{-3}K^{-1}$
Volumetric heat capacity of the liquid phase	C_w	4180000 $Jm^{-3}K^{-1}$
Tortuosity coefficient in the liquid and vapor phases	τ_w, τ_g	0.67
Dispersivity	Λ	0

6.1.1 Comparison with the analytical solution of Zimmermann et al. (1967)

Zimmermann et al. (1967) conducted experiments and provided an analytical solution for the isotope transport in a homogeneous saturated soil column with the initial isotope ratio (isotopic composition), $R_\infty(\delta_\infty)$, evaporating at a steady rate, E_s, into the atmosphere of constant humidity, h_a, air temperature T_a, and isotope ratio (isotopic composition), $\delta_{ia}^v(R_{ia}^v)$, under isothermal

conditions at a soil temperature T_z. Table 3 provides all relevant parameter values. Under steady-state conditions, the stable isotope profile can be explained by the balance between the upward convective flux (evaporation) and the downward diffusion flux of the isotope:

$$E_s(R_i^l - R_\infty) = D_i^{l*} \mathrm{d}R_i^l/\mathrm{d}z \quad (49)$$

where R_i^l is the isotope ratio at depth z (z is equal to zero at the soil surface and it is positive downwards).

The above equation can be solved to get:

$$R_i^l = R_\infty + (R_0 - R_\infty)\, exp(-z/z_l) \quad (50)$$

where R_0 is the isotope ratio at the soil surface, and z_l is the characteristic length given by:

$$z_l = D_i^{l*}/E_s \quad (51)$$

If one reports the isotope ratio in Eq. (50) in the δ notation (‰) using Eq. (2), we can get:

$$\delta_i^l = \delta_\infty + (\delta_0 - \delta_\infty)\, exp(-z/z_l) \quad (52)$$

where δ_0 (δ_i^l) are isotopic compositions at the soil surface and at depth z, respectively.

The isotopic composition at the soil surface δ_0 can be calculated using a variant of the Craig-Gordon model as follows (*Barnes and Allison*, 1983):

$$\alpha_i^* (1 + \delta_0) - h_a'(1 + \delta_{ia}^v) = (1 - h_a')\alpha_i^k (1 + \delta_\infty) \quad (53)$$

The analytical solution for ^{18}O is:

$$\delta^{18}O \ (‰) = 31.9exp^{(-16.949z)} \cdot 1000‰ \quad (54)$$

and for ^{2}H is:

$$\delta\ ^2H \ (‰) = 67exp^{(-16.667z)} \cdot 1000‰ \quad (55)$$

In the HYDRUS numerical simulation, transport parameters were the same as those in the analytical solution. Both the upper and lower BCs were set to a constant water pressure head for water flow. The soil water pressure head was assumed to be 1 cm at the surface and 109.15 cm at the bottom. This BC allowed for a permanent water supply at the bottom of the soil column and kept the soil saturated while maintaining the steady evaporation rate E_s. Both the upper and lower BCs were set to solute flux BCs for isotope transport. The surface solute flux in this example referred to the evaporation flux for water isotopes E_i calculated by the Craig-Gordon model (Eq.

(7)). The bottom isotope flux was calculated assuming that the isotope ratio (isotopic composition) of supply water was the same as the initial values, $R_\infty(\delta_\infty)$. No heat transport was considered in this example.

Figs. 3a and 3b show an excellent agreement between the numerical and analytical solutions using a fine spatial discretization. Fig. S2 shows a comparison between the analytical and numerical solutions' results using different spatial discretizations. The maximum differences between the analytical and numerical solutions in the ^{18}O isotopic composition profiles were 0.21‰ (coarse), 0.20‰ (medium), and 0.20‰ (fine). The maximum differences between the analytical and numerical solutions in the ^{2}H isotopic composition profiles were 0.46‰ (coarse), 0.43‰ (medium), and 0.43‰ (fine). We may conclude that the isotope transport module can produce in this example accurate isotope profiles using all considered spatial discretization schemes.

Water that has experienced evaporation fractionation plots below the global/local meteoric water line (GMWL/LMWL) in dual-isotope plots. The occurrence of kinetic fractionation results in an evaporation line with a slope much smaller than those of GMWL/LMWL (*Sprenger et al.*, 2016a). The "line conditioned excess" (LC-excess) is the difference between the $\delta\,^{2}H$ from a water sample and a linear transformation of the $\delta\,^{2}H$ from a given GMWL/LMWL (*Landwehr and Coplen*, 2006). The more negative it is, the stronger the kinetic fractionation is (*Sprenger et al.*, 2017). The dual-isotope plot (Fig. 3c) has a slope of about 2.09, which is much smaller than that (8.20) of the global meteoric water line (GMWL). The LC-excess profile (calculated by Eq. (A6)) shows the opposite trend to the isotopic composition profiles and is negative in the entire soil profile (Fig. 3d). These results suggest that kinetic fractionation also occurs. This is reasonable given the fact that kinetic fractionation factor (α_i^k) is not equal to one (Table 3).

Table 3. Values of all variables used in the analytical solution of *Zimmermann et al.* (1967).

Parameter	**Value**
E_s	1.003×10^{-5} $kgm^{-2}s^{-1}$
$T_a,\ T_z$	303.15 K (30 ℃)

h_a	0.2	
n_k	1	
	for ^{18}O	for ^{2}H
D_i^{l*}	5.91×10^{-10} m^2/s	6.01×10^{-10} m^2/s
Z_l	0.059 m	0.060 m
δ_{ia}^v	-14‰	-100‰
R_{ia}^v	0.001977127	0.000140184
δ_∞	0‰	0‰
R_∞	0.0020052	0.00015576
δ_0	31.9‰	67‰
R_0	0.002063684	0.00016733
α_i^*	0.9911	0.9311
α_i^k	1.031885	1.016363

1

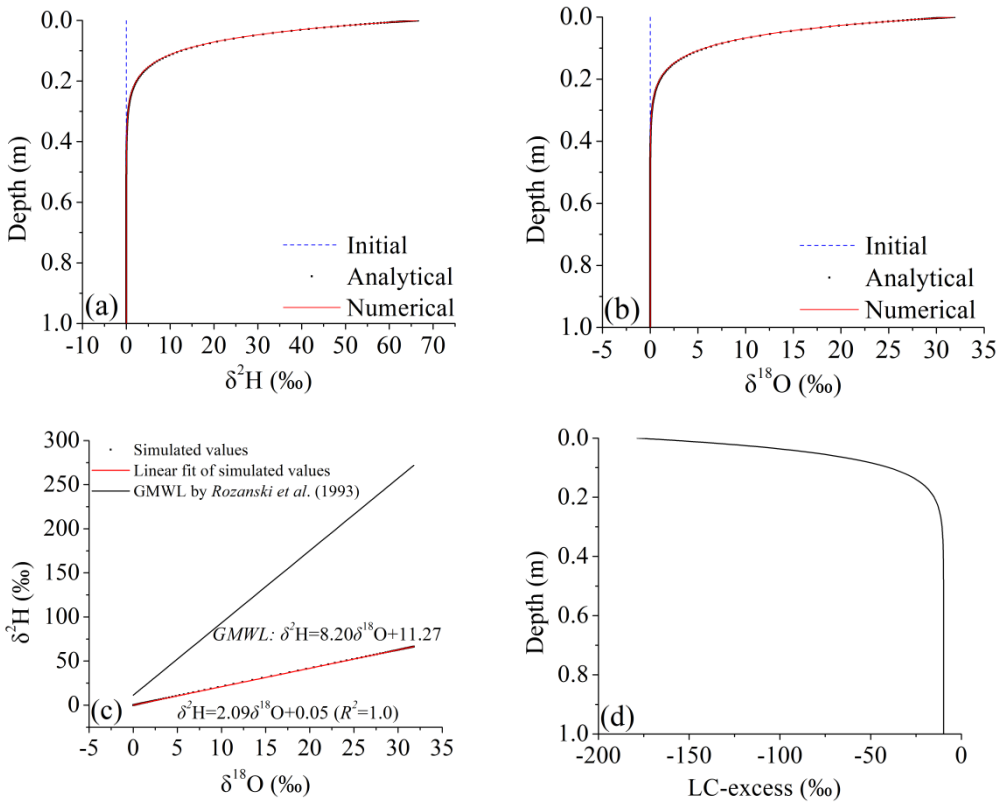

2 Figure 3. Comparison of analytical and numerical solutions for profiles of (a) the ^{2}H isotopic
3 composition and (b) the ^{18}O isotopic composition, (c) the dual-isotope plot of simulated values,
4 and (d) the LC-excess profile for isothermal saturated soil under steady evaporation.

6.1.2 Comparison with the analytical solution of Barnes and Allison (1984)

Barnes and Allison (1984) proposed an analytical solution for evaporation from unsaturated soil under steady and nonisothermal conditions. Conditions were the same as for the steady-state saturated case above, except that the initial pressure head was set to 0 in the entire soil profile, nonisothermal conditions were considered, and evaporation occurred at a different rate. Table 4 gives the values of all parameters required in this problem. Under steady-state conditions (i.e., at 250 days of the simulation), the stable isotope profile can be explained by the balance between the upward convective flux (evaporation) and the downward diffusion flux of the isotope both in the liquid and vapor phases:

$$-E_s = \rho_w(q_l + q_v) = \rho_w q_l - D^{v*} \cdot \frac{d(H_r \cdot \rho_{sat}^v)}{dz} \tag{56}$$

$$-E_s R_\infty = q_i^l + q_i^v = (\rho_w q_l R_i - \rho_w D_i^{l*} \frac{dR_i^l}{dz}) - D_i^{v*} \frac{d(H_r \cdot \rho_{sat}^v . R_i^v)}{dz} \tag{57}$$

where D^{v*} is the effective dispersion coefficient of the light isotope in soil water vapor, E_s is the steady state evaporation rate and H_r is the relative humidity of the soil air phase at a certain depth. H_r can be calculated by Eq. (5), while the matric potential h_s and temperature T_s at the soil surface should be replaced by corresponding values at a certain soil depth. If we expand the derivative form of the vapor flux ($-D^{v*} \cdot \frac{d(H_r \cdot \rho_{sat}^v)}{dz}$) in Eq. (56), we can easily find that it describes the sum of the isothermal ($K_{vh} \frac{\partial h}{\partial z}$) and nonisothermal ($K_{vT} \frac{\partial T}{\partial z}$) terms in Eq. (22). If we expand the derivative form of the isotope diffusion flux in the soil water vapor ($-D_i^{v*} \frac{d(H_r \cdot \rho_{sat}^v . R_i^v)}{dz}$) in Eq. (57), we can easily find out that it describes the sum of the convection ($\beta_i^* q_v C_i^l$) and diffusion ($-D_i^{v*} \frac{\partial \beta_i^* C_i^l}{\partial z}$) terms in Eq. (25). That is to say, vapor convection within the soil is also a diffusive process (*Haverd et al.*, 2010).

If we define characteristic lengths z_l and z_v as follows:

$$z_l = \rho_w D^{l*} / E_s \tag{58}$$

$$z_v = \frac{D^{v*}\rho_{sat}^{v}}{E_s} \tag{59}$$

We can then get:

$$(\rho_w q_v)/E_s = -D^{v*}\frac{d(H_r \cdot \rho_{sat}^{v})}{dz}/E_s = -H_r z_v \frac{d[ln(H_r \cdot \rho_{sat}^{v})]}{dz} \tag{60}$$

$$\begin{aligned} q_i^v/E_s &= -D_i^{v*}\frac{d(H_r \cdot \rho_{sat}^{v} R_i^v)}{dz}/E_s \\ &= -H_r z_v R_i^l \alpha_i^*/\alpha_i^k \frac{d[ln(H_r \rho_{sat}^{v} \alpha_i^* R_i^l)]}{dz} \end{aligned} \tag{61}$$

$$\begin{aligned} q_i^l/E_s &= (\rho_w q_l R_i^l - \rho_w D_i^{l*}\frac{dR_i^l}{dz})/E_s \\ &= \rho_w q_l R_i^l/E_s - z_l \sigma_i R_i^l \frac{d[ln(R_i^l)]}{dz} \end{aligned} \tag{62}$$

Combining these equations gives:

$$\begin{aligned} &H_r z_v R_i^l\{(1-\alpha_i^*/\alpha_i^k)\frac{d[\ln(H_r \rho_{sat}^{v})]}{dz} - \alpha_i^*/\alpha_i^k \frac{d\left[\ln\left(\alpha_i^* R_i^l\right)\right]}{dz}\} \\ &= R_i^l - R_\infty + z_l \sigma_i \frac{dR_i^l}{dz} \end{aligned} \tag{63}$$

where D^{l*} is the effective dispersion coefficient of the light isotope in soil water, and σ_i is a constant depending on the isotope species (see Appendix A).

According to the relationship between R and δ values shown in Eq. (2), the analytical solution can be further simplified and given by the differential equation as follows:

$$\begin{aligned} &\frac{d\delta_i^l}{dz} + (z_l + H_r z_v)^{-1}\left(\delta_i^l - \delta_\infty\right) \\ &= H_r z_v (z_l + H_r z_v)^{-1}(\alpha_i^k - \alpha_i^*) \times \frac{d}{dz}[\ln(H_r \rho_{sat}^{v}(\alpha_i^k \\ &- \alpha_i^*))] \end{aligned} \tag{64}$$

This is a semi-analytical solution. It can only be solved once we prescribe the isotopic composition of soil water at the surface and solve the water flow and heat transport equations, which will provide soil temperatures, pressure heads, and water contents. In the HYDRUS numerical simulation, transport parameters were the same as those in the analytical solution. The constant pressure head (equal to 0) was adopted in the numerical simulation as the lower BC for soil water flow. The new water flow BC, which calculates actual evaporation as a function of

potential evaporation (E_p) and the difference in humidities between the air and the soil surface (Eq. (35)) was used at the upper atmospheric boundary. The solute flux was used as the lower BC for isotope transport (automatically calculated from its isotopic composition equal to δ_∞ and the bottom water flux). The stagnant BC for volatile solutes was used at the upper boundary for isotope transport. The surface solute flux referred to the evaporation flux for water isotopes E_i calculated by the Craig-Gordon model (Eq. (7)). The temperature BC was used for heat transport at both boundaries.

Figs. 4e and 4f show an excellent agreement between the analytical and numerical solutions using a fine spatial discretization, despite a slight overestimation of the peak isotopic composition by HYDRUS-1D. Fig. S3 compares the analytical and numerical solutions obtained using different spatial discretizations. The maximum differences (at the evaporation front) between the analytical and numerical solutions in the ^{18}O isotopic composition profiles were 24.88‰ (coarse discretization), 3.74‰ (medium), and 0.88‰ (fine). The maximum differences between the analytical and numerical solutions in the ^{2}H isotopic composition profiles were 34.68‰ (coarse), 8.40‰ (medium), and 3.67‰ (fine). This means that in this example, the isotope transport module can produce relatively well isotope profiles as long as an appropriate spatial discretization is used. The isotopic composition profiles have maximum values at a depth of 2 cm, which corresponds with the water content/matric potential/temperature profiles inflection points (Figs. 4a, 4b, and 4c). This is also the evaporation front location, where the upward soil water flux changes from the liquid to vapor flux (Fig. 4d).

The dual-isotope plots (Fig. 4g) have slopes of about 2.66 and 1.62 in the vapor and liquid dominant zones (VDZ, LDZ), respectively, which are far smaller than those of the GMWL. The LC-excess profile shows the opposite trend to the isotopic composition profiles and is negative in the entire soil profile (Fig. 4h). These results suggest that kinetic fractionation also occurs. This is reasonable since the kinetic fractionation factor (α_i^k) is not equal to one when n_k is one (Table 4).

Table 4. Values of all variables used in the analytical solution of *Barnes and Allison* (1984).

Parameter	Value
E_p	2.0×10^{-4} kgm^{-2}s^{-1}
E_s	1.043×10^{-5} kgm^{-2}s^{-1}
T_a	313.15 K (40 ℃)
T_z	$T_z = 20(1+\exp(-20z)) + 273.15\ \ K$
h_a	0.2
δ_{ia}^v	-14‰ for ^{18}O and -100‰ for ^{2}H
δ_∞	0‰ for ^{18}O and 0‰ for ^{2}H
n_k	1

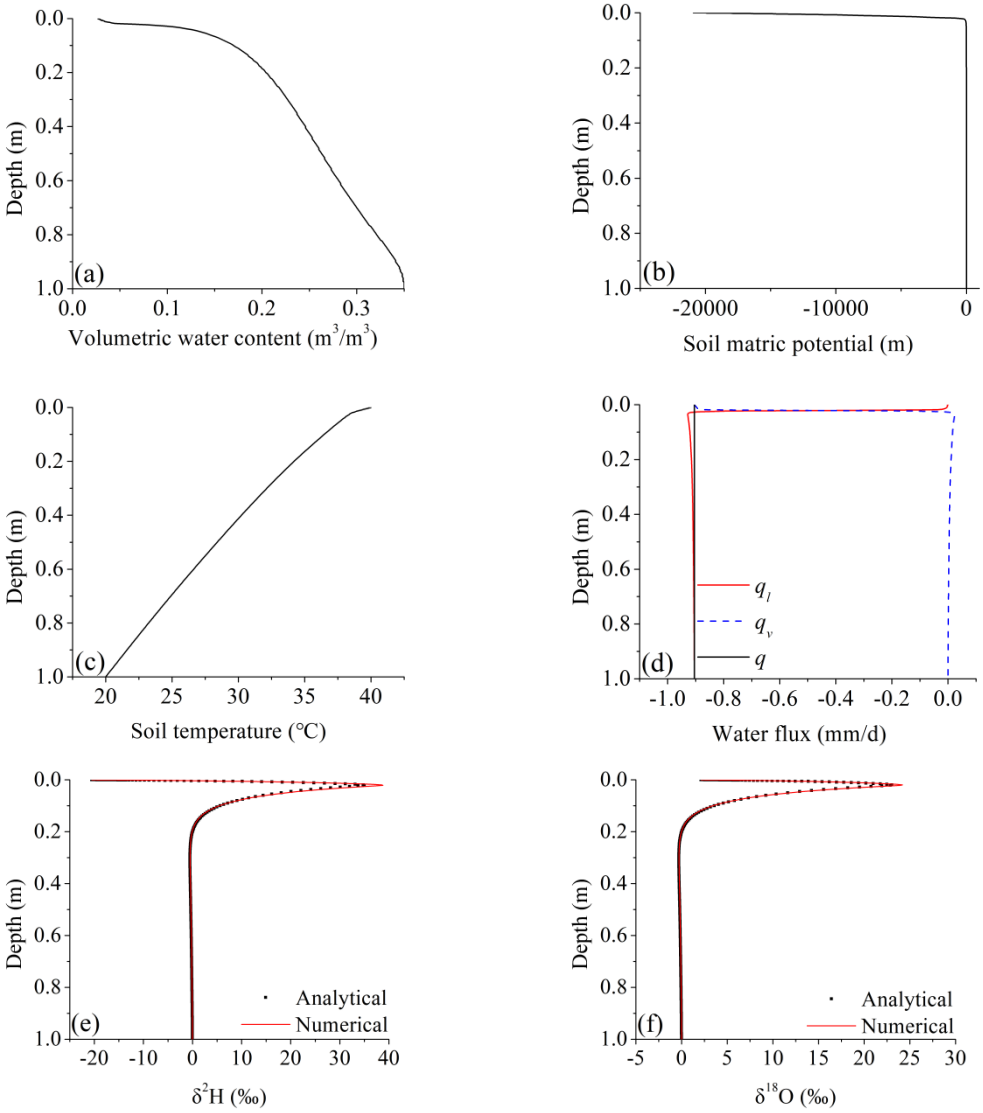

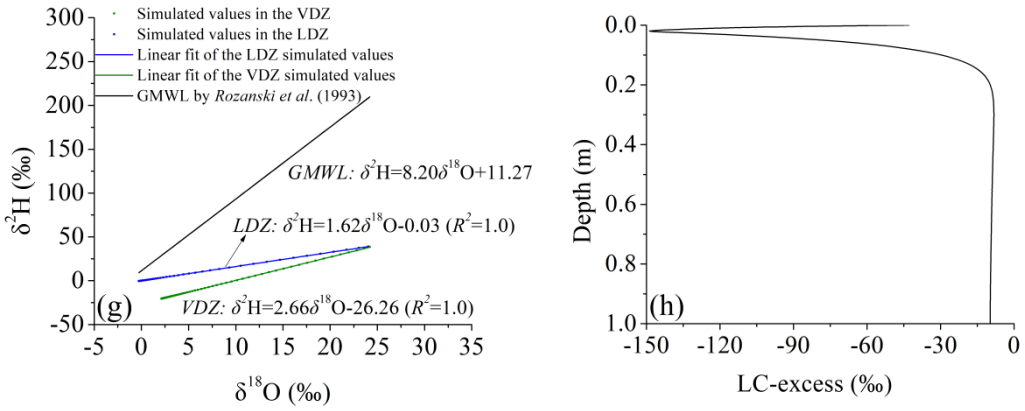

Figure 4. Comparison of the results of analytical and numerical solutions for nonisothermal unsaturated soils under steady evaporation. Vertical profiles of (a) the soil water content, (b) the matric potential, (c) the soil temperature, (d) the water fluxes (liquid, q_l, vapor, q_v, and total, q; negative values represent evaporation), (e) the ^{2}H isotopic composition, (f) the ^{18}O isotopic composition, (g) the dual-isotope plot of the simulated values and (h) the LC-excess profile. "VDZ" and "LDZ" represent the vapor and liquid-dominant zones, respectively.

6.1.3 Plausibility tests

The soil was initially saturated and under hydrostatic conditions (the soil water pressure head was equal to -0.01 m at the top and linearly increased to 0.99 m at the bottom). The initial isotopic composition, δ_∞, and soil temperature, T_z, in the soil column were uniform (i.e., the same at all depths). Water was evaporating from the soil column into an atmosphere with temperature, T_a, relative humidity, h_a, and isotopic composition, δ_{ia}^v. All relevant parameters are summarized in Table 5 (*Mathieu and Bariac*, 1996; *Melayah et al.*, 1996; *Braud et al.*, 2005a). In the HYDRUS numerical simulation, zero water and isotope fluxes were adopted as the lower BCs. The new water flow BC, which calculates actual evaporation as a function of potential evaporation (E_p) and the difference in humidities between the air and the soil surface (Eq. (35)) was used at the upper atmospheric boundary. The stagnant BC for volatile solutes was used at the upper boundary for isotope transport. The surface solute flux referred to the evaporation flux for water isotopes E_i calculated by the Craig-Gordon model (Eq. (7)). No heat transport was considered in this example.

The plausibility test conditions are listed in Table 6. The impacts of four parameters on isotopic composition profiles were considered, including the equilibrium fractionation factor, α_i^*,

the kinetic fractionation factor, α_i^k, which affects the molecular diffusion coefficient of the isotope *i* in free air, D_i^v, the molecular diffusion coefficient of the isotope *i* in free water, D_i^l, and the isotopic composition of atmospheric vapor, δ_{ia}^v. Equations from *Majoube* (1971) and *Mathieu and Bariac* (1996) were used to calculate the equilibrium α_i^* and kinetic fractionation factor α_i^k, respectively, for tests in which they were not equal to 1. The molecular diffusion coefficients of the isotope *i* in free water (air) D_i^{lo} (D_i^v) [L^2T^{-1}] were calculated by Eqs. (A3~A5). These values were then used to calculate the effective dispersion coefficients for the isotope *i* in soil water (vapor), D_i^{l*} (D_i^{v*}), based on Eqs. (33~34). The steady vertical isotopic composition profiles at the end of the 250-day simulation are shown in Fig. 5.

Test 1: Equilibrium and kinetic fractionation factors (α_i^*, α_i^k) are set to one, and molecular diffusion coefficient of the isotope *i* in free water (D_i^{lo}) is set to zero. In other words, evaporation fractionation and diffusion in the liquid phase are neglected. The isotopic composition of the atmospheric water vapor is set equal to that of the initial soil water δ_∞. This results in uniform isotopic compositions in soil water throughout the soil profile (equal to δ_∞) as expected.

Test 2: Test 2 is the same as Test 1, except that the isotopic composition of the atmospheric water vapor is set to a low value δ_{ia}^v. Isotope diffusion in soil water vapor due to the concentration gradient between the free atmosphere and soil results in increased isotopic compositions of liquid and vapor phases within the soil as depth increases, given the linear relationship between them (Eq. (32)). The isotopic composition of surface soil water is close to that of the atmospheric water vapor δ_{ia}^v and increases gradually with depth to its initial value δ_∞.

Test 3: Test 3 is the same as Test 1, except that equilibrium isotopic fractionation is turned on (i.e., α_i^* is not equal to one). Equilibrium fractionation between soil water and soil water vapor moves lighter water molecules from the liquid phase into the vapor phase, which causes isotopic enrichment of the remaining soil water. However, this enrichment rate is different between regions above and below 5 cm (i.e., the evaporation front, as seen in Figs. 5a and 5b) due to different vapor fluxes. Above 5 cm, the vapor flux is approximately constant with depth, and thus the effect of

equilibrium fractionation does not differ too much with depth. This results in a slow transition from the isotopic composition of soil water towards the surface value. Below 5 cm, the isotopic composition of soil water increases rapidly towards the 5-cm depth due to the increased upward vapor flux (Fig. 5b).

Test 4: Test 4 is the same as Test 3, except that the isotopic composition of the atmospheric water vapor is reset to a low value δ_{ia}^{v}. This shifts the isotopic composition of surface soil water close to δ_{ia}^{v}, similarly as in Test 2. This surface effect, combined with increasing enrichment from the soil bottom towards the soil surface (as discussed in Test 3), leads to the simulated maximum of the isotopic composition profile.

Test 5: Test 5 is the same as Test 4, except that diffusion in the liquid phase is turned on (i.e., D_i^{l0} is not equal to zero). Since diffusion in the liquid phase causes spreading or dispersion of the solute front (*Radcliffe and Šimůnek*, 2018), this test produces a smaller peak of the isotopic composition profile.

Test 6: Test 6 is the same as Test 5, except that the kinetic fractionation at the surface is turned on (i.e., α_i^k is not equal to one), and the molecular diffusion coefficient of the isotope *i* in free air is set to its real value D_i^v (smaller than D^v as seen in Eq. (12)). The smaller molecular diffusion coefficient in free air results in increased kinetic fractionation, by decreasing the removal of heavy isotopes through the vapor flux. This increases isotopic enrichment in the remaining soil water, leading to a larger peak of the isotopic composition profile than in Test 5.

As for dual-isotope plots, Test 6 has slopes far smaller than that of the global meteoric water line (GMWL) in both liquid- (LDZ) and vapor-dominant (VDZ) zones (Fig. S4d). The line conditioned excess (LC-excess) profile shows the opposite trends to the isotopic composition profiles and is always negative (Fig. S5). These suggest that kinetic fractionation also occurs. This is reasonable given the fact that the kinetic fractionation factor (α_i^k) is not equal to one in Test 6 (Table 6). For Tests 3~5, the dual-isotope plots of both the LDZ and VDZ (Figs. S4a, S4b, and S4c) have slopes of about 6.55~7.80, which are much closer to that of the GMWL. This is

reasonable since the kinetic fractionation factor is equal to one in Tests 3~5 (Table 6), and thus only equilibrium fractionation occurs. These slopes are not exactly equal to that of GMWL, especially for the VDZ, where the exchange with the atmosphere is more significant. However, the LC-excess values in Tests 3~5 are almost a constant low value (about -10‰) throughout the soil profile, compared to much more negative values in Test 6 (Fig. S5). This again verifies that only equilibrium fractionation occurs in Tests 3~5.

Overall, the slopes of dual-isotope plots with kinetic fractionation are much smaller than those without consideration (Fig. 3c, Fig. 4g, and Fig. S4). The LC-excesses at the surface layer (about 0~50 cm) are much more negative than in other depths (Fig. 3d, Fig. 4h, and Fig. S5). This indicates that the fractionation at the surface layer is more significant. These conclusions are also consistent with those in *Sprenger et al.* (2016a). Therefore, the isotope transport module is accurate also from the perspectives of dual-isotope plots and LC-excess values.

Table 5. Values of all variables used in the plausibility tests.

Parameter	**Value**	
E_p	1.005 $\times 10^{-4}$ kg/m^2/s	
E_s	2.568 $\times 10^{-6}$ kg/m^2/s	
T_a, T_z	303.15 K (30 ℃)	
h_a	0.2	
	for ^{18}O	for ^{2}H
δ_{ia}^{v}	-15‰	-112‰
δ_{∞}	-8‰	-65‰
D_i^{lo}	2.520$\times 10^{-9}$ m^2/s	2.562$\times 10^{-9}$ m^2/s
D_i^{v}	2.529$\times 10^{-5}$ m^2/s	2.568$\times 10^{-5}$ m^2/s

Table 6. Plausibility tests' conditions.

Test	$\boldsymbol{\alpha_i^*}$	$\boldsymbol{\alpha_i^k}$	$\boldsymbol{D_i^v}$	$\boldsymbol{D_i^{lo}}$	$\boldsymbol{\delta_{ia}^v}$
1	1	1	D^v	0	δ_{∞}
2	1	1	D^v	0	δ_{ia}^v
3	α_i^*	1	D^v	0	δ_{∞}
4	α_i^*	1	D^v	0	δ_{ia}^v
5	α_i^*	1	D^v	D_i^{l0}	δ_{ia}^v

6	α_i^*	α_i^k	D_i^v	D_i^{l0}	δ_{ia}^v

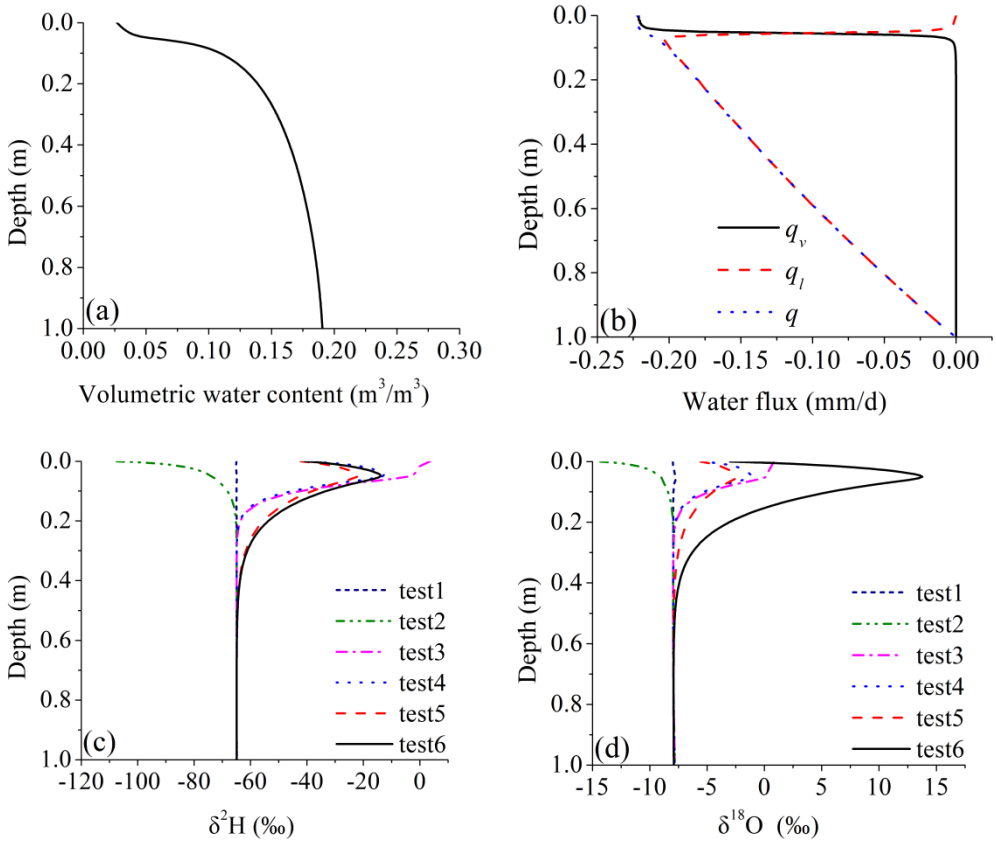

Figure 5. Vertical profiles of (a) the soil water content, (b) the water fluxes (liquid, q_l, vapor, q_v, and total, q; negative values represent evaporation), (c) the ^{2}H isotopic composition, and (d) the ^{18}O isotopic composition in plausibility tests 1-6 at 250 d.

6.2 Evaluation against the experiment data

6.2.1 The transport of isotopes

The dataset is from *Stumpp et al.* (2012) (available https://www.pc-progress.com/en/Default.aspx?h1d-lib-isotope). The field experiment was conducted in a humid region located at the research area of the HBLFA Raumberg-Gumpenstein in Gumpenstein, Austria, with a mean annual temperature of 6.9 °C and mean annual precipitation of 1035 mm. The cylindrical lysimeter (with a depth of 1.5 m and a surface area of 1 m^2) was embedded in a rainfed agricultural field planted with winter wheat and fertilized with liquid cattle slurry (the lysimeter 3 in *Stumpp et al.* (2012)). The isotopic composition of precipitation and lysimeter

seepage water were measured on the event and weekly intervals, respectively, from May 2002 to February 2007 (1736 days in total). The temporal distribution of precipitation, evapotranspiration, temperature, air humidity during the simulation period are provided in Fig. S6. More details about other data collection and measurements can be found in *Stumpp et al.* (2012).

The final optimized soil hydraulic and solute transport parameters reported in *Stumpp et al.* (2012) (Table S2) were used in the numerical simulations reported below. The atmospheric (with a surface layer) and seepage face boundary conditions were used for water flow at the upper and lower boundaries, respectively. The temperature BC was used for heat transport at both boundaries. The solute flux and zero concentration gradient BCs were used for isotope transport at the upper and lower boundaries, respectively. The isotope ratio of the evaporation flux was automatically used in HYDRUS to calculate the isotope evaporation flux at the upper boundary corresponding to the water flux. To investigate the sensitivity of the simulation results to the upper boundary conditions for isotope transport, the relevant parameters (R_E, R_a) of different evaporation fractionation models (*Stumpp et al.,* 2012; the Craig-Gordon model, and the Gonfiantini model) were adjusted and implemented. Their impacts on the simulation results under different assumptions (with and without fractionation) were discussed. Since kinetic fractionation can be neglected in humid zones (*Horita et al.,* 2008), only equilibrium fractionation was considered in this example (i.e., $n_k = 0$). Fig. 6 shows the comparison between ^{18}O isotopic compositions of the lysimeter seepage water simulated by *Stumpp et al.* (2012) and using the Gonfiantini and Craig-Gordon models for a system that neglects vapor flow. The Nash-Sutcliffe efficiency (NSE) and determination coefficient (R^2) are shown in Table 7.

The water samples from the lysimeter seepage water plot on the LMWL (Fig. 5 of *Stumpp et al.,* 2012), indicating negligible fractionation. Therefore, the measured data are closest to the simulations that do not consider fractionation, as *Stumpp et al.* (2012) did. In this model. the isotope ratio of the evaporation flux (R_E) is the same as that of the surface soil water (R_L) (i.e., $R_E = R_L$).

In the Gonfiantini model, R_E is α_i^* times of R_L. As can be seen in Fig. 6, the measured values are close to the values simulated by the Gonfiantini model in case of no fractionation (i.e., $\alpha_i^* = 1;\ n_k = 0;\ R_E = R_L$, which produces the same results as *Stumpp et al*., 2012) for most of the simulation period. In the end, during about 1150~1500 days, the measured values are close to those simulated considering equilibrium fractionation (i.e., $\alpha_i^* = \alpha_i^*;\ n_k = 0;\ R_E = \alpha_i^* R_L$).

To obtain a better agreement between the simulation results and measurements using the Craig-Gordon model, the early atmospheric isotope ratio R_a should correspond to Eq. S9 (i.e., $R_a = \frac{(\alpha_i^* - 1 + h_a)\cdot R_L}{h_a}$), while the late R_a should correspond to Eq. S7 (i.e., $R_a = \alpha_i^* \cdot R_L$). Therefore, in the Craig-Gordon model method, an approximate estimate of R_a using Eq. (S10) was used for the entire simulation period to calculate R_E under equilibrium fractionation assumption (i.e., $\alpha_i^* = \alpha_i^*;\ n_k = 0;\ R_a = \frac{(\alpha_i^* - 1 + h_a + h_a\cdot\alpha_i^*)\cdot R_L}{2h_a}$). More details can be found in the Supplementary Material.

The Craig-Gordon model has obtained relatively satisfactory simulation results (NSE=0.19; R^2=0.30) compared to the Gonfiantini model (NSE=-0.52; R^2=0.25) in the case of equilibrium fractionation. The significant differences between the values simulated by the Gonfiantini and Craig-Gordon models emphasize the considerable impact of R_a on the simulation results due to its effect on R_E. However, the model performance is worse than when fractionation is neglected (NSE=0.24; R^2=0.37). This also indirectly validates the assumption of *Stumpp et al.* (2012) not to consider evaporation fractionation in their analysis of data from this humid zone. However, this does not rule out errors due to an inaccurate estimation of R_a used in the simulation. We note that the final optimized soil hydraulic and solute transport parameters reported in *Stumpp et al.* (2012) were used in the numerical simulations. This parameter set was estimated based on the assumption that there was no fractionation, which may not be optimal when fractionation is present. This may also explain the best agreement of the *Stump et al.* (2012) simulation with the measurements.

However, even under the no-fractionation assumption, this agreement is not very good, likely due to some uncontrollable factors in the field experiments.

The isotopic compositions and overall temporal variation trends simulated using the Gonfiantini or Craig-Godron models considering fractionation are consistent with measured data and the *Stumpp et al.* (2012) simulation without considering fractionation. This is because evaporation fractionation will not change isotopic composition trends when evaporation is much smaller than the sum of precipitation and soil water storage, and the equilibrium fractionation factor is close to 1. However, the selection of the atmospheric isotope ratio R_a can affect the fluctuation amplitude of the isotope time series by affecting R_E. The isotopic composition of discharge simulated by all models remains the same during the first 150 days because only water initially in the profile (and thus not affected by the upper BC treatment) reaches the bottom during this time. Water infiltrating at the beginning of the simulation starts arriving at the bottom after about 150 days when isotopic compositions simulated by different models with different assumptions start deviating. From this point forward, differences in simulated discharge isotopic compositions reflect different treatments of the upper BC.

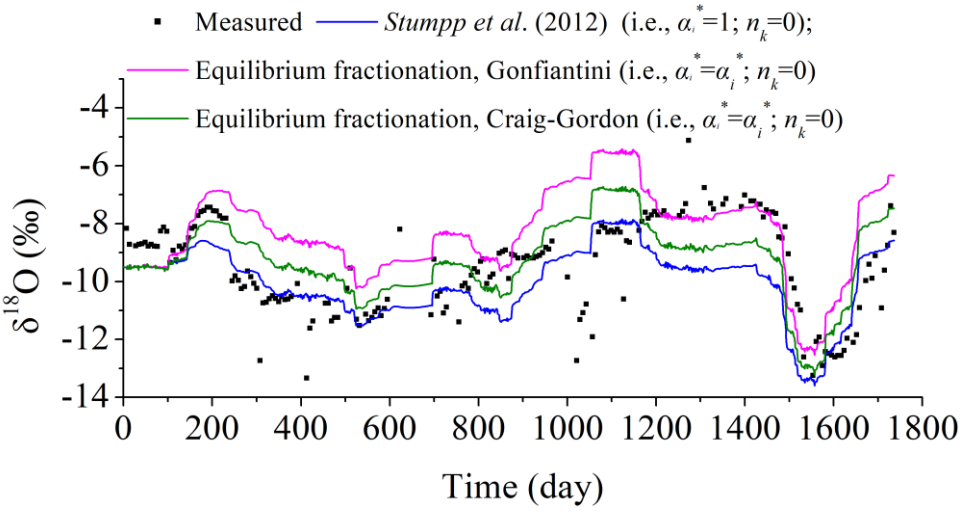

Figure 6. Simulated $\delta^{18}O$ in the seepage water at the bottom of the lysimeter when equilibrium fractionation was (i.e., $\alpha_i^* = \alpha_i^*$; $n_k = 0$) or was not (i.e., $\alpha_i^* = 1$; $n_k = 0$) considered for the *Stumpp et al.* (2012) dataset using the Gonfiantini and Craig-Gordon evaporation fractionation models.

Table 7. Statistics of the model performance.

Indicator	no fractionation, *Stumpp et al.* (2012) (i.e., $\alpha_i^* = 1;\ \ n_k = 0$)	Equilibrium fractionation, the Gonfiantini model (i.e., $\alpha_i^* = \alpha_i^*;\ \ n_k = 0$)	Equilibrium fractionation, the Craig-Gordon model (i.e., $\alpha_i^* = \alpha_i^*;\ \ n_k = 0$)
NSE	0.24	-0.52	0.19
R^2	0.37	0.25	0.30

6.2.2 Particle tracking

The input parameters, w_{Stand} and w_{Prec} (discussed in Section 4.3), of the particle tracking module (PTM) were set equal to 2 and 10 cm, respectively. Fig. 7 shows the spatial-temporal distribution of particles during the 5-year simulation. There are 48 particles in total, among which 18 particles (P1-P18) were initially in the soil profile, while the next 26 particles (P19~P44) were released at the soil surface, passed through the lysimeter, and left at the bottom. Finally, the last 4 particles (P45-P48) were released at the soil surface and remained in the soil profile at the end of the simulation.

The particle trajectories suddenly drop during periods with many rainfall events and slowly decrease or even rise during periods with limited rainfall (Fig. 7). Particles move downward faster during wet seasons and slow down during dry seasons. Particles move down sharply after heavy rainfalls, reflecting piston flow's typical characteristics. Particles released right before the wet season move down faster than those released right before the dry season.

The transit times of these particles, and corresponding velocities, were calculated (given in Table S4. and shown in Fig. 7c). The mean recharge transit time and velocity are 276.1 days and 6.0 mm/day, respectively. These values are slightly different from those calculated by *Stumpp et al.* (2012) using the peak displacement method. The mean recharge transit time (250 days) and velocity (6.0 mm/day) of soil water were estimated by *Stumpp et al.* (2012) by comparing the convective shift in the isotope peaks of the input (precipitation during 2005~2006) and output (lysimeter discharge) and considering dispersion effects. This difference may also be due to

different rainfall events selected for these calculations. *Stumpp et al.* (2012) selected precipitation events from 2005~2006 since, only during this period, there was pronounced and distinct correspondence between the isotopic peaks in precipitation and lysimeter discharge. Since particles move faster during the period with many precipitation events, the peak displacement method is likely to overestimate the flow velocity compared to particle tracking. Overall, the two approaches' results are similar, which shows the particle tracking model's applicability.

However, the peak displacement method is not applicable when there are no pronounced peaks or a distinct correspondence between the input and output peaks. The particle tracking module can be used under such circumstances and overcome this shortcoming of the peak-displacement method, thus expanding the possibility of calculating transit times.

To verify the new particle tracking module, we conducted simple mass balance calculations based on the results of the numerical solution of the Richards equation in HYDRUS-1D. The amount of water in the soil profile when the particle leaves the transport domain (W_{t_final}) should be equal to the amount of water applied at the soil surface (infiltration) since its release, reduced by evaporation and root water uptake from the soil between the particle and the soil surface:

$$W_{t_{final}} = \int_{t_{init}}^{t_{final}} \left(i(t) - e(t) - \int_{0}^{z_p(t)} s(z,t) dz \right) dt \qquad (65)$$

where t_{init} and t_{final} are times when the particle is released at the soil surface and when it leaves at the soil profile bottom, respectively. The mass balance calculations carried out according to (65) are given in Table S4, indicating an almost perfect match and validating the particle tracking module.

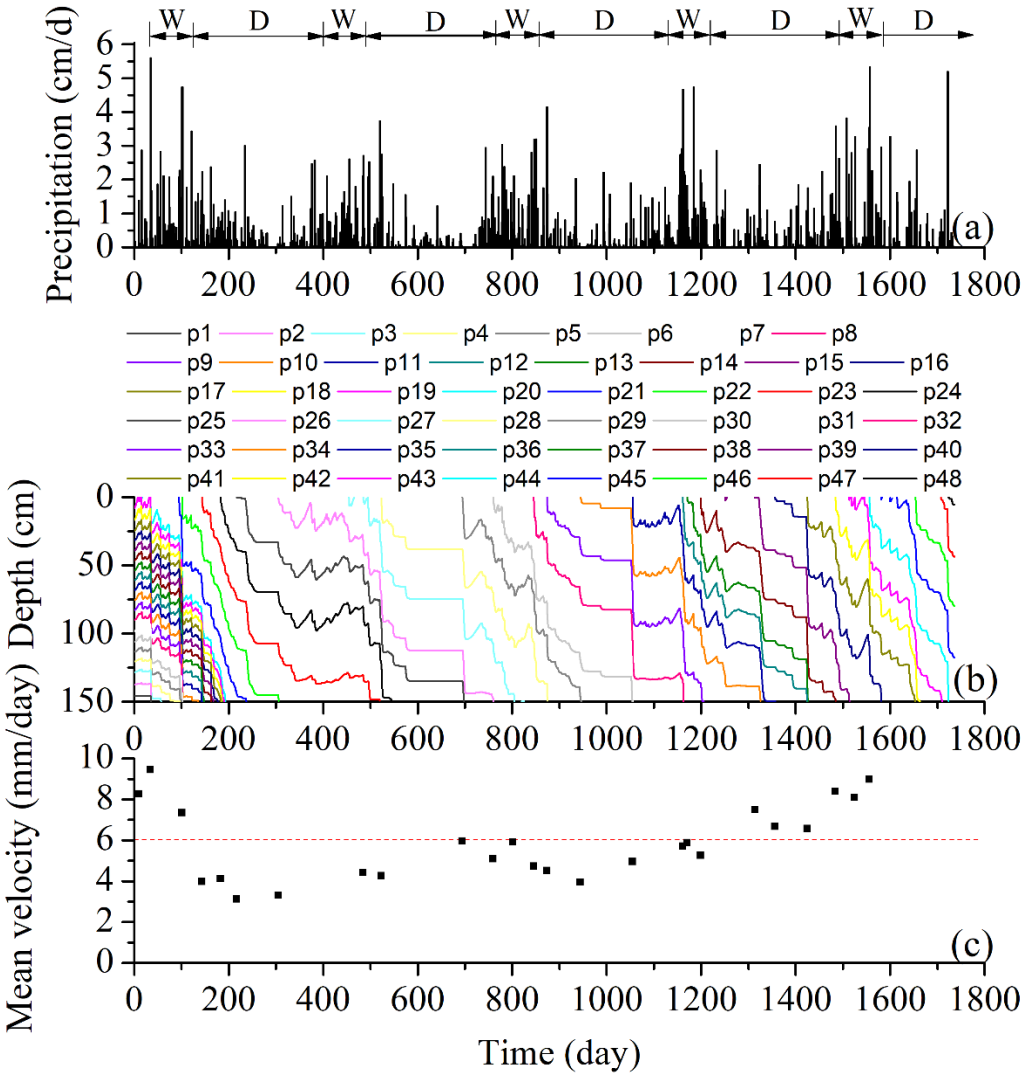

Figure 7. Precipitation (a), spatial-temporal distribution of particles (b), and mean particle velocity (c) (simulated by the Particle Tracking Module) for the *Stumpp et al.* (2012) dataset. "W" and "D" represent wet and dry seasons, respectively.

6.3 Discussion and future work

Modeling water flow and solute transport in the critical zone requires an accurate estimation of soil hydraulic and solute transport parameters. Combining different types of observed data to calibrate water flow and solute transport models has been found to improve model parameterization. For example, *Sprenger et al.* (2015) demonstrated that a combination of stable isotope profiles and soil moisture time series allowed for a better model calibration for solute transport, water flow, and root water uptake parameters. *Groh et al.* (2018) determined the soil

hydraulic parameters and the longitudinal dispersivity for multiple lysimeters using two-step and bi-objective optimization strategies. They concluded that the bi-objective strategy, combining water content, matric potential, and tracer data, was the best parameter estimation strategy. *Mattei et al.* (2020) showed that it is possible to use only water content and stable isotope profiles measured at one time to accurately calibrate the model for groundwater recharge estimation. However, using stable isotope data at different soil depths at different times can improve the model calibration (*Mattei et al.*, 2020).

The new isotope transport module in HYDRUS-1D can simulate continuous space-time dynamics of stable water isotope concentrations of soil water. Whether the impact of consideration of evaporation fractionation will propagate into the inversion of soil hydraulic and solute transport parameters is unknown. Future work will include analyzing field datasets collected in arid regions or laboratory experiments of *Braud et al*. (2009), where evaporation fractionation plays a vital role and depth-dependent observations are available. Sensitivity analyses and parameter inversions will be conducted to evaluate the new isotope transport model further.

The assumption of well-mixed water in the soil is in contrast with the recent "two water world" (TWW) hypothesis that water in the soil should be split into two pools that are isotopically different (*Berry et al.*, 2018; *Brooks et al.*, 2010; *McDonnell*, 2014). The first pool (the mobile soil water pool) often replenishes groundwater and has isotopic composition close to that of the infiltrating water. The second pool (the immobile soil water pool) is supposed to be composed of tightly bound water enriched by evaporation that resides in the soil's capillary space, some of which can be used by plants. Many isotopic measurements support the hypothesis of the widespread existence of TWW and demonstrate that some sampling methods (e.g., suction lysimeters) are likely to obtain the mobile water, while others (e.g., centrifugation, cryogenic or toluene distillation) are prone to sample all soil water (e.g., *Figueroa-Johnson et al.*, 2007*; Geris et al.*, 2015; *Goldsmith et al.*, 2012; *Knighton et al.*, 2019; *Oerter and Bowen*, 2017; *Zhao et al.*, 2016).

The TWW hypothesis was formulated based on two assumptions (*Vargas et al.*, 2017). The first is that there is no mass exchange between the mobile and immobile waters. The second is that plant water uptake does not discriminate against ^{2}H or ^{18}O and thus does not affect the isotopic composition of soil water. However, recent studies have shown that mass exchange between mobile and immobile waters (e.g., *Oshun et al.*, 2016; *Vargas et al.*, 2017) and isotopic fractionation may occur during plant water uptake (e.g., *Barbeta et al.*, 2019; *Poca et al.*, 2019). On the other hand, there is accumulating evidence showing that the equilibrium isotope fractionation between pore water and water vapor within the soil is significantly different from that between liquid and water vapor for free water surface due to complex hydrophilic interactions between soil pore surface and water molecules (e.g., *Chen et al.*, 2016; *Gaj and McDonnell*, 2019; *Lin and Horita*, 2016; *Lin et al.*, 2018; *Oerter et al.*, 2014). However, how waters of different mobility alter the isotopic composition of soil water is little understood and seldom accounted for in isotope transport modeling (*Sprenger et al.*, 2018).

The standard version of HYDRUS-1D can consider a series of physical nonequilibrium flow and transport models (e.g., dual-porosity and dual-permeability), and the same conceptualization can be applied to simulate isotope transport. These nonequilibrium flow and transport models will be used in our future studies to evaluate the impacts of physical nonequilibrium on isotope transport modeling and transit time calculations for TWW systems.

7 Summary and conclusions

This study presents a model, which can simultaneously solve the coupled equations describing the movement of water, heat, and stable isotopes. It is based on the HYDRUS-1D model, to which the isotope transport and particle tracking modules were added. The comparisons with analytical solutions, plausibility tests under saturated/unsaturated and isothermal/nonisothermal conditions, and field validation demonstrate the model's accuracy and robustness. Transit times calculated by the particle tracking module (PTM) are similar to those evaluated by the peak

displacement method, which validates the use of the water flow-based PTM as an alternative tool to isotope transport-based methods.

As compared with existing isotope models, our approach enables many thousands of current HYDRUS users to efficiently operate the new model while using various advanced HYDRUS software features, including flexible dynamic boundary conditions, equilibrium and nonequilibrium water flow, parameter optimization routines, and the well-designed user-friendly GUI (*Šimůnek et al.,* 2016), while also providing higher computational efficiency. For example, the SiSPAT model always calculates both water flow and heat transport, even when the soil system is isothermal. Our model simulates only water flow for isothermal systems, improving numerical efficiency. The new particle tracking module provides the HYDRUS-1D users with an additional tool for assessing transit times. The developed model represents a comprehensive tool to numerically investigate many important research problems involving isotope transport processes and establishes a more solid foundation for applying stable isotope tracing in the critical zone.

Software and Data Availability

Hardware: PC

Software: HYDRUS-1D

Developed Module Names: Isotope transport and particle tracking modules

Contact Person: Jirka Šimůnek, Tiantian Zhou. Email: jiri.simunek@ucr.edu; tzhou035@ucr.edu

Address: Department of Environmental Sciences, University of California Riverside, CA 92521, United States

Data: The dataset for each example has already been listed, or the link is provided in the article.

Code: The executable program is available upon request.

Acknowledgments

This research was financially supported by the Multistate W4188 program. We appreciate editors and reviewers for their constructive comments on this manuscript.

Appendix A

The density of the saturated water vapor ρ_{sat}^{v} (kg/m^3) depending on temperature T (K) is calculated as follows:

$$\rho_{sat}^{v} = 10^{-3}\frac{\exp(31.3716 - \frac{6014.79}{T} - 7.92495\cdot 10^{-3}\cdot T)}{T} \quad \text{(A1)}$$

The density of the water vapor ρ_v is the product of the density of the saturated water vapor ρ_{sat}^{v} (kg/m^3) and relative humidity H_r [-]:

$$\rho_v = H_r \cdot \rho_{sat}^{v} \quad \text{(A2)}$$

The molecular diffusion coefficient of the isotope *i* in free water D_i^{lo} [L^{2}T^{-1}] is expressed as a function of temperature T (K):

$$D_i^{lo} = \sigma_i \cdot 10^{-9}\, exp(-\frac{535400}{T^2} + \frac{1393.3}{T} + 2.1876) \quad \text{(A3)}$$

where σ_i is a constant depending on the isotope species (0.98331 for HDO and 0.96691 for $H_2{}^{18}O$).

The molecular diffusion of the isotope *i* in free air D_i^{v} [L^{2}T^{-1}] is expressed as a function of temperature T (K):

$$D_i^{v} = D^{v}/b_i \quad \text{(A4)}$$

$$D^{v} = 2.12\cdot 10^{-5}(\frac{T}{273.16})^2 \quad \text{(A5)}$$

where b_i is the ratio of the molecular diffusion coefficients of light and heavy water (isotopes) in free air (1.0166 for HDO and 1.0324 for $H_2{}^{18}O$ as discussed in Eq. (12)).

For the verification examples in this study, the GMWL defined by *Rozanski et al.* (1993) was used. The LC-excess was calculated as follows:

$$LC-excess = (\delta\,{}^2H - 8.2\delta^{18}O - 11.27)/1.15 \quad \text{(A6)}$$

References

Allen, S.T., J.W. Kirchner, S. Braun, R.T.W. Siegwolf, and G.R. Goldsmith, Seasonal origins of soil water used by trees, *Hydrology and Earth System Sciences*, *23*(2), pp. 1199-1210, doi:10.5194/hess-23-1199-2019, 2019.Asadollahi, M., C. Stumpp, A. Rinaldo, and P. Benettin, Transport and water age dynamics in soils: a comparative study of spatially integrated and spatially explicit models, *Water Resources Research*, *56*(3), pp. 17, doi:10.1029/2019wr025539, 2020.

Auriault, J.L., and P.M. Adler, Taylor dispersion in porous media: Analysis by multiple scale expansions, *Advances in Water Resources*, *18*(4), pp. 217-226, doi:10.1016/0309-1708(95)00011-7, 1995.

Barbeta, A., S.P. Jones, L. Clave, L. Wingate, T.E. Gimeno, B. Frejaville, S. Wohl, and J. Ogee, Unexplained hydrogen isotope offsets complicate the identification and quantification of tree water sources in a riparian forest, *Hydrology and Earth System Sciences*, *23*(4), pp. 2129-2146, doi:10.5194/hess-23-2129-2019, 2019.

Barnes, C.J., and G.B. Allison, The distribution of deuterium and ^{18}O in dry soils: 1. Theory, *Journal of Hydrology*, *60*(1-4), pp. 141-156, doi:10.1016/0022-1694(83)90018-5, 1983.

Barnes, C.J., and G.B. Allison, The distribution of deuterium and ^{18}O in dry soils: 3. Theory for non-isothermal water movement, *Journal of Hydrology*, *74*(1-2), pp. 119-135, doi:10.1016/0022-1694(84)90144-6, 1984.

Berry, Z.C., J. Evaristo, G. Moore, M. Poca, K. Steppe, L. Verrot, H. Asbjornsen, L.S. Borma, M. Bretfeld, P. Herve-Fernandez, M. Seyfried, L. Schwendenmann, K. Sinacore, L. De Wispelaere, and J. McDonnell, The two water worlds hypothesis: Addressing multiple working hypotheses and proposing a way forward, *Ecohydrology*, *11*(3), pp. 10, doi:10.1002/eco.1843, 2018.

Braud, I., SiSPAT User's Manual Version 3.0. Laboratoire d'Étude des Transferts en Hydrologie et Environnement, Grenoble, France, pp. 106, 2000.

Braud, I., SiSPAT User's Manual Update, Version 4.0, pp. 13, 2002.

Braud, I., T. Bariac, J.P. Gaudet, and M. Vauclin, SiSPAT-Isotope, a coupled heat, water and stable isotope (HDO and $H_2{}^{18}O$) transport model for bare soil. Part I. Model description and first verifications, *Journal of Hydrology*, *309*(1-4), pp. 277-300, doi:10.1016/j.jhydrol.2004.12.013, 2005a.

Braud, I., T. Bariac, M. Vauclin, Z. Boujamlaoui, J.P. Gaudet, P. Biron, and P. Richard, SiSPAT-Isotope, a coupled heat, water and stable isotope (HDO and $H_2{}^{18}O$) transport model for bare soil. Part II. Evaluation and sensitivity tests using two laboratory data sets, *Journal of Hydrology*, *309*(1-4), pp. 301-320, doi:10.1016/j.jhydrol.2004.12.012, 2005b.

Braud, I., P. Biron, T. Bariac, P. Richard, L. Canale, J.P. Gaudet, and M. Vauclin, Isotopic composition of bare soil evaporated water vapor. Part I: RUBIC IV experimental setup and results, *Journal of Hydrology*, *369*(1-2), pp. 1-16, doi:10.1016/j.jhydrol.2009.01.034, 2009.

Braud, I., A.C. Dantasantonino, M. Vauclin, J.L. Thony, and P. Ruelle, A simple soil-plant-atmosphere transfer model(SiSPAT) development and field verification, *Journal of Hydrology*, *166*(3-4), pp. 213-250, doi:10.1016/0022-1694(94)05085-c, 1995.

Brinkmann, N., S. Seeger, M. Weiler, N. Buchmann, W. Eugster, and A. Kahmen, Employing stable isotopes to determine the residence times of soil water and the temporal origin of water taken up by Fagus sylvatica and Picea abies in a temperate forest, *New Phytologist*, *219*(4), pp. 1300-1313, doi:10.1111/nph.15255, 2018.

Brooks, J.R., H.R. Barnard, R. Coulombe, and J.J. McDonnell, Ecohydrologic separation of water between trees and streams in a Mediterranean climate, *Nature Geoscience*, *3*(2), pp. 100-104, doi:10.1038/ngeo722, 2010.

Brooks, R., and A. Corey, Hydraulic properties of porous media, *Hydrology Papers, No. 3*. Colorado State University, Fort Collins, Colo, pp., 1964.

Brown, C.R., M. Kandelous, F. Sartori, C. Collins, and F. Spurlock, Modeling variation in 1,3-dichloropropene emissions due to soil conditions and applicator practices, *Science of the Total Environment*, *678*, pp. 768-779, doi:10.1016/j.scitotenv.2019.04.414, 2019.

Burdine, N.T., Relative permeability calculations from pore size distribution data, *Transactions of the American Institute of Mining and Metallurgical Engineers*, *198*, pp. 71-78, 1953.

Chen, G., K. Auerswald, and H. Schnyder, H-2 and O-18 depletion of water close to organic surfaces, *Biogeosciences*, *13*(10), pp. 3175-3186, doi:10.5194/bg-13-3175-2016, 2016.

Corneo, P.E., Kertesz, M.A., Bakhshandeh, S., Tahaei, H., Barbour, M.M., Dijkstra, F.A., 2018. Studying root water uptake of wheat genotypes in different soils using water delta 18O stable isotopes. *Agriculture Ecosystems & Environment*, 264: 119-129. doi:10.1016/j.agee.2018.05.007.

Chung, S.O., and R. Horton, Soil heat and water-flow with a partial surface mulch, *Water Resources Research*, *23*(12), pp. 2175-2186, doi:10.1029/WR023i012p02175, 1987.

Craig, H., Isotopic variations in meteoric waters, *Science*, *133*(346), pp. 1702-1703, doi:10.1126/science.133.3465.1702, 1961.

Craig, H., and L. Gordon, Deuterium and oxygen 18 variations in the ocean and the marine atmosphere, Stable Isotopes in Oceanographic Studies and Paleotemperatures E, *Proceedings of the Third Spoleto Conference*, Spoleto, Italy, pp. 9-130, 1965.

De Vries, D.A., Thermal properties of soils, In Physics of Plant Environment, Wijk, R.W.v. (Ed.), North Holland, Amsterdam, pp. 210-235, 1963.

Figueroa-Johnson, M.A., J.A. Tindall, and M. Friedel, A comparison of O-18 delta composition of water extracted from suction lysimeters, centrifugation, and azeotropic distillation, *Water Air Soil Pollut.*, *184*(1-4), pp. 63-75, doi:10.1007/s11270-007-9399-8, 2007.

Fry, B., Stable Isotope Ecology, 521, Springer, New York, NY, pp., 2006.

Gaj, M., and J.J. McDonnell, Possible soil tension controls on the isotopic equilibrium fractionation factor for evaporation from soil, *Hydrological Processes*, *33*(11), pp. 1629-1634, doi:10.1002/hyp.13418, 2019.

Gat, J., Isotope Hydrology: A Study of the Water Cycle, 6, World Scientific, pp., 2010.

Gehrels, J.C., J.E.M. Peeters, J.J. De Vries, and M. Dekkers, The mechanism of soil water movement as inferred from O-18 stable isotope studies, *Hydrological Sciences Journal*, *43*(4), pp. 579-594, doi:10.1080/02626669809492154, 1998.

Geris, J., D. Tetzlaff, J. McDonnell, J. Anderson, G. Paton, and C. Soulsby, Ecohydrological separation in wet, low energy northern environments? A preliminary assessment using different soil water extraction techniques, *Hydrological Processes*, *29*(25), pp. 5139-5152, doi:10.1002/hyp.10603, 2015.

Goldsmith, G.R., L.E. Munoz-Villers, F. Holwerda, J.J. McDonnell, H. Asbjornsen, and T.E. Dawson, Stable isotopes reveal linkages among ecohydrological processes in a seasonally dry tropical montane cloud forest, *Ecohydrology*, *5*(6), pp. 779-790, doi:10.1002/eco.268, 2012.

Gonfiantini, R., Standards for stable isotope measurements in natural compounds, *Nature*, *271*(5645), pp. 534-536, doi:10.1038/271534a0, 1978.

Gonfiantini, R., Environmental isotopes in lake studies, *Handbook of environmental isotope geochemistry*, *2*, pp. 113-168, 1986.

Gonfiantini, R., L.I. Wassenaar, L. Araguas-Araguas, and P.K. Aggarwal, A unified Craig-Gordon isotope model of stable hydrogen and oxygen isotope fractionation during fresh or saltwater evaporation, *Geochimica Et Cosmochimica Acta*, *235*, pp. 224-236, doi:10.1016/j.gca.2018.05.020, 2018.

Groh, J., C. Stumpp, A. Lucke, T. Putz, J. Vanderborght, and H. Vereecken, Inverse Estimation of Soil Hydraulic and Transport Parameters of Layered Soils from Water Stable Isotope and Lysimeter Data, *Vadose Zone Journal*, *17*(1), pp. 19, doi:10.2136/vzj2017.09.0168, 2018.

Haverd, V., and M. Cuntz, Soil-Litter-Iso: A one-dimensional model for coupled transport of heat, water and stable isotopes in soil with a litter layer and root extraction, *Journal of Hydrology*, *388*(3-4), pp. 438-455, doi:10.1016/j.jhydrol.2010.05.029, 2010.

Horita, J., K. Rozanski, and S. Cohen, Isotope effects in the evaporation of water: a status report of the Craig-Gordon model, *Isotopes in Environmental and Health Studies*, *44*(1), pp. 23-49, doi:10.1080/10256010801887174, 2008.

Horita, J., and D.J. Wesolowski, Liquid-vapor fractionation of oxygen and hydrogen isotopes of water from the freezing to the critical temperature, *Geochimica Et Cosmochimica Acta*, *58*(16), pp. 3425-3437, doi:10.1016/0016-7037(94)90096-5, 1994.

Jury, W.A., W.F. Spencer, and W.J. Farmer, Behavior assessment model for trace organics in soil, 1. Model description, *Journal of Environment Quality*, *12*(4), pp. 558-564, doi:10.2134/jeq1983.00472425001200040025x, 1983.

Jury, W.A., G. Sposito, and R.E. White, A transfer-function model of solute transport through soil.1. Fundamental concepts, *Water Resources Research*, *22*(2), pp. 243-247, doi:10.1029/WR022i002p00243, 1986.

Kendall, C., and J.J. McDonnell, Isotope Tracers in Catchment Hydrology, Elsevier, pp., 2012.

Kim, M., L.A. Pangle, C. Cardoso, M. Lora, T.H.M. Volkmann, Y.D. Wang, C.J. Harman, and P.A. Troch, Transit time distributions and StorAge Selection functions in a sloping soil lysimeter with time-varying flow paths: Direct observation of internal and external transport variability, *Water Resources Research*, *52*(9), pp. 7105-7129, doi:10.1002/2016wr018620, 2016.

Knighton, J., V. Souter-Kline, T. Volkman, P.A. Troch, M. Kim, C. Harman, C. Morris, B. Buchanan, and M.T. Walter, Seasonal and topographic variations in ecohydrological separation within a small, temperate, snow-influenced catchmet, *Water Resources Research*, *55*(8), pp. 6417-6435, doi:10.1029/2019wr025174, 2019.

Kool, D., Agam, N., Lazarovitch, N., Heitman, J.L., Sauer, T.J., Ben-Gal, A., 2014. A review of approaches for evapotranspiration partitioning. *Agricultural and Forest Meteorology*, 184: 56-70. DOI:10.1016/j.agrformet.2013.09.003.

Landwehr, J., and T. Coplen, Line-conditioned excess: a new method for characterizing stable hydrogen and oxygen isotope ratios in hydrologic systems, *International conference on isotopes in environmental studies*, IAEA Vienna, pp. 132-135, 2006.

Lin, Y., and J. Horita, An experimental study on isotope fractionation in a mesoporous silica-water system with implications for vadose-zone hydrology, *Geochimica Et Cosmochimica Acta*, *184*, pp. 257-271, doi:10.1016/j.gca.2016.04.029, 2016.

Lin, Y., J. Horita, and O. Abe, Adsorption isotope effects of water on mesoporous silica and alumina with implications for the land-vegetation-atmosphere system, *Geochimica Et Cosmochimica Acta*, *223*, pp. 520-536, doi:10.1016/j.gca.2017.12.021, 2018.

Ma, Y., Song, X.F., 2016. Using stable isotopes to determine seasonal variations in water uptake of summer maize under different fertilization treatments. *Science of the Total Environment*, 550: 471-483. DOI:10.1016/j.scitotenv.2016.01.148.

Majoube, M., Oxygen-18 and deuterium fractionation between water and steam, *Journal De Chimie Physique Et De Physico-Chimie Biologique*, *68*(10), pp. 1423-1436, doi:10.1051/jcp/1971681423, 1971.

Maloszewski, P., S. Maciejewski, C. Stumpp, W. Stichler, P. Trimborn, and D. Klotz, Modelling of water flow through typical Bavarian soils: 2. Environmental deuterium transport, *Hydrological Sciences Journal*, *51*(2), pp. 298-313, doi:10.1623/hysj.51.2.298, 2006.

Mathieu, R., and T. Bariac, A numerical model for the simulation of stable isotope profiles in drying soils, *Journal of Geophysical Research-Atmospheres*, *101*(D7), pp. 12685-12696, doi:10.1029/96jd00223, 1996.

Mattei, A., P. Goblet, F. Barbecot, S. Guillon, Y. Coquet, and S.T. Wang, Can Soil Hydraulic Parameters be Estimated from the Stable Isotopic composition of Pore Water from a Single Soil Profile?, *Water*, *12*(2), pp. 19, doi:10.3390/w12020393, 2020.

McDonnell, J.J., The two water worlds hypothesis: ecohydrological separation of water between streams and trees?, *Wiley Interdisciplinary Reviews-Water*, *1*(4), pp. 323-329, doi:10.1002/wat2.1027, 2014.

Melayah, A., L. Bruckler, and T. Bariac, Modeling the transport of water stable isotopes in unsaturated sails under natural conditions. 1. Theory, *Water Resources Research*, *32*(7), pp. 2047-2054, doi:10.1029/96wr00674, 1996a.

Melayah, A., L. Bruckler, and T. Bariac, Modeling the transport of water stable isotopes in unsaturated soils under natural conditions. 2. Comparison with field experiments, *Water Resources Research*, *32*(7), pp. 2055-2065, doi:10.1029/96wr00673, 1996b.

Merlivat, L., Molecular diffusivities of $H_2{}^{16}O$, $HD^{16}O$, and $H_2{}^{18}O$ in gases, *Journal of Chemical Physics*, *69*(6), pp. 2864-2871, doi:10.1063/1.436884, 1978.

Millington, R., and J.P. Quirk, Permeability of porous solids, *Transactions of the Faraday Society*, *57*(8), pp. 1200-1207, doi:10.1039/tf9615701200, 1961.

Moldrup, P., T. Olesen, D.E. Rolston, and T. Yamaguchi, Modeling diffusion and reaction in soils .7. Predicting gas and ion diffusivity in undisturbed and sieved soils, *Soil Sci.*, *162*(9), pp. 632-640, doi:10.1097/00010694-199709000-00004, 1997.

Mueller, M.H., A. Alaoui, C. Kuells, H. Leistert, K. Meusburger, C. Stumpp, M. Weiler, and C. Alewell, Tracking water pathways in steep hillslopes by delta ^{18}O depth profiles of soil water, *Journal of Hydrology*, *519*, pp. 340-352, doi:10.1016/j.jhydrol.2014.07.031, 2014.

Oerter, E., K. Finstad, J. Schaefer, G.R. Goldsmith, T. Dawson, and R. Amundson, Oxygen isotope fractionation effects in soil water via interaction with cations (Mg, Ca, K, Na) adsorbed to phyllosilicate clay minerals, *Journal of Hydrology*, *515*, pp. 1-9, doi:10.1016/j.jhydrol.2014.04.029, 2014.

Oerter, E.J., and G. Bowen, In situ monitoring of H and O stable isotopes in soil water reveals ecohydrologic dynamics in managed soil systems, *Ecohydrology*, *10*(4), pp. 13, doi:10.1002/eco.1841, 2017.

Oshun, J., W.E. Dietrich, T.E. Dawson, and I. Fung, Dynamic, structured heterogeneity of water isotopes inside hillslopes, *Water Resources Research*, *52*(1), pp. 164-189, doi:10.1002/2015wr017485, 2016.

Philip, J.R., Evaporation, moisture and heat field in the soil, *Journal of Meteorology*, *14*(4), pp. 354-366, doi:10.1175/1520-0469(1957)014<0354:eamahf>2.0.co;2, 1957.

Philip, J., and D. De Vries, Moisture movement in porous materials under temperature gradients, *Eos, Transactions American Geophysical Union*, *38*(2), pp. 222-232, doi:10.1029/TR038i002p00222, 1957.

Poca, M., O. Coomans, C. Urcelay, S.R. Zeballos, S. Bode, and P. Boeckx, Isotope fractionation during root water uptake by Acacia caven is enhanced by arbuscular mycorrhizas, *Plant and Soil*, *441*(1-2), pp. 485-497, doi:10.1007/s11104-019-04139-1, 2019.

Quade, M., N. Bruggemann, A. Graf, J. Vanderborght, H. Vereecken, and Y. Rothfuss, Investigation of kinetic isotopic fractionation of water during bare soil evaporation, *Water Resources Research*, *54*(9), pp. 6909-6928, doi:10.1029/2018wr023159, 2018.

Radcliffe, D.E., and J. Šimůnek, Soil Physics with HYDRUS: Modeling and Applications, CRC Press, pp., 2018.

Rinaldo, A., P. Benettin, C.J. Harman, M. Hrachowitz, K.J. McGuire, Y. van der Velde, E. Bertuzzo, and G. Botter, Storage selection functions: A coherent framework for quantifying how catchments store and release water and solutes, *Water Resources Research*, *51*(6), pp. 4840-4847, doi:10.1002/2015wr017273, 2015.

Ross, P.J., Modeling soil water and solute transport - Fast, simplified numerical solutions, *Agronomy Journal*, *95*(6), pp. 1352-1361, doi:10.2134/agronj2003.1352, 2003.

Rothfuss, Y., and M. Javaux, Reviews and syntheses: Isotopic approaches to quantify root water uptake: a review and comparison of methods, *Biogeosciences*, *14*(8), pp. 2199-2224, doi:10.5194/bg-14-2199-2017, 2017.

Rozanski, K., L. Araguás-Araguás, and R. Gonfiantini, Isotopic patterns in modern global precipitation, *Climate change in continental isotopic records*, *78*, pp. 1-36, 1993.

Saito, H., J. Šimůnek, and B.P. Mohanty, Numerical analysis of coupled water, vapor, and heat transport in the vadose zone, *Vadose Zone Journal*, *5*(2), pp. 784-800, doi:10.2136/vzj2006.0007, 2006.

Shurbaji, A.R.M., and F.M. Phillips, A numerical model for the movement of H_2O, $H_2{}^{18}O$, and ^2HHO in the unsaturated zone, *Journal of Hydrology*, *171*(1-2), pp. 125-142, doi:10.1016/0022-1694(94)02604-a, 1995.

Šimůnek, J., Numerical simulation of the transport processes in soil (in Czech, English abstract), *Vodohosp. Čas.*, *39*(1), pp. 20-34, 1991.

Šimůnek, J., M. Sejna, H. Saito, M. Sakai, and M.T. van Genuchten, The HYDRUS-1D Software Package for Simulating the One-Dimensional Movement of Water, Heat, and Multiple Solutes in Variably Saturated Media, Version 4.0, *HYDRUS Software Series 3*, Department of Environmental Sciences, University of California Riverside, Riverside, California, USA, pp., 2008.

Šimůnek, J., M.T. van Genuchten, and M. Sejna, Recent developments and applications of the HYDRUS computer software packages, *Vadose Zone Journal*, *15*(7), pp. 25, doi:10.2136/vzj2016.04.0033, 2016.

Soderberg, K., S.P. Good, L.X. Wang, and K. Caylor, Stable isotopes of water vapor in the vadose zone: a review of measurement and modeling techniques, *Vadose Zone Journal*, *11*(3), pp. 14, doi:10.2136/vzj2011.0165, 2012.

Sprenger, M., H. Leistert, K. Gimbel, and M. Weiler, Illuminating hydrological processes at the soil-vegetation-atmosphere interface with water stable isotopes, *Reviews of Geophysics*, *54*(3), pp. 674-704, doi:10.1002/2015rg000515, 2016a.

Sprenger, M., S. Seeger, T. Blume, and M. Weiler, Travel times in the vadose zone: Variability in space and time, *Water Resources Research*, *52*(8), pp. 5727-5754, doi:10.1002/2015wr018077, 2016b.

Sprenger, M., D. Tetzlaff, and C. Soulsby, Soil water stable isotopes reveal evaporation dynamics at the soil-plant-atmosphere interface of the critical zone, *Hydrology and Earth System Sciences*, *21*(7), pp. 3839-3858, doi:10.5194/hess-21-3839-2017, 2017.

Sprenger, M., D. Tetzlaff, J. Buttle, H. Laudon, H. Leistert, C.P.J. Mitchell, J. Snelgrove, M. Weiler, and C. Soulsby, Measuring and modeling stable isotopes of mobile and bulk soil water, *Vadose Zone Journal*, *17*(1), pp. 18, doi:10.2136/vzj2017.08.0149, 2018.

Sprenger, M., T.H.M. Volkmann, T. Blume, and M. Weiler, Estimating flow and transport parameters in the unsaturated zone with pore water stable isotopes, *Hydrology and Earth System Sciences*, *19*(6), pp. 2617-2635, doi:10.5194/hess-19-2617-2015, 2015.

Spurlock, F., B. Johnson, A. Tuli, S.D. Gao, J. Tao, F. Sartori, R.J. Qin, D. Sullivan, M. Stanghellini, and H. Ajwa, Simulation of fumigant transport and volatilization from tarped broadcast applications, *Vadose Zone Journal*, *12*(3), pp. 10, doi:10.2136/vzj2013.03.0056, 2013a.

Spurlock, F., J. Šimůnek, B. Johnson, and A. Tuli, Sensitivity analysis of soil fumigant transport and volatilization to the atmosphere, *Vadose Zone Journal*, *12*(2), pp. 12, doi:10.2136/vzj2012.013, 2013b.

Stumpp, C., and P. Maloszewski, Quantification of preferential flow and flow heterogeneities in an unsaturated soil planted with different crops using the environmental isotope delta O-18, *Journal of Hydrology*, *394*(3-4), pp. 407-415, doi:10.1016/j.jhydrol.2010.09.014, 2010.

Stumpp, C., W. Stichler, M. Kandolf, and J. Šimůnek, Effects of land cover and fertilization method on water flow and solute transport in five lysimeters: A long-term study using stable water isotopes, *Vadose Zone Journal*, *11*(1), pp. 14, doi:10.2136/vzj2011.0075, 2012.

Tetzlaff, D., C. Birkel, J. Dick, J. Geris, and C. Soulsby, Storage dynamics in hydropedological units control hillslope connectivity, runoff generation, and the evolution of catchment transit time distributions, *Water Resources Research*, *50*(2), pp. 969-985, doi:10.1002/2013wr014147, 2014.

Timbe, E., D. Windhorst, P. Crespo, H.G. Frede, J. Feyen, and L. Breuer, Understanding uncertainties when inferring mean transit times of water trough tracer-based lumped-parameter models in Andean tropical montane cloud forest catchments, *Hydrology and Earth System Sciences*, *18*(4), pp. 1503-1523, doi:10.5194/hess-18-1503-2014, 2014.

van Genuchten, M.T., A closed-form equation for predicting the hydraulic conductivity of unsaturated soils, *Soil Science Society of America Journal*, *44*(5), pp. 892-898, doi:10.2136/sssaj1980.03615995004400050002x, 1980.

Vargas, A.I., B. Schaffer, Y.H. Li, and L.D.L. Sternberg, Testing plant use of mobile vs immobile soil water sources using stable isotope experiments, *New Phytologist*, *215*(2), pp. 582-594, doi:10.1111/nph.14616, 2017.

Wang, J., Lu, N., Fu, B.J., 2019. Inter-comparison of stable isotope mixing models for determining plant water source partitioning. *Science of the Total Environment*, 666: 685-693. DOI:10.1016/j.scitotenv.2019.02.262.

Xiao, W., Wei, Z.W., Wen, X.F., 2018. Evapotranspiration partitioning at the ecosystem scale using the stable isotope method-A review. *Agricultural and Forest Meteorology*, 263: 346-361. DOI:10.1016/j.agrformet.2018.09.005.

Zhao, P., X.Y. Tang, P. Zhao, and J.L. Tang, Dynamics of water uptake by maize on sloping farmland in a shallow Entisol in Southwest China, *Catena*, *147*, pp. 511-521, doi:10.1016/j.catena.2016.08.001, 2016.

Zheng, C., J. Šimůnek, Y. Lu, X. Liu, C. Shi, and H. Li, Monitoring and modeling the coupled movement of water, vapor, and energy in arid areas, *Journal of Hydrology*, *590*, pp. 125528, 2020.

Zimmermann, U., D. Ehhalt, and K. Münnich, Soil-water movement and evapotranspiration: Changes in the isotopic composition of the water, *Proceedings of the symposium of Isotopes in Hydrology.*, IAEA, Vienna, Austria, pp. 567-584, 1967.